GLO-Roots: an imaging platform enabling multidimensional characterization of soil-grown root systems

Rubén Rellán-Álvarez[1, 9], Guillaume Lobet[2], Heike Lindner[1, 8], Pierre-Luc Pradier[1, 8, 10], Jose Sebastian[1, 8], Muh-Ching Yee[1], Yu Geng[1, 7], Charlotte Trontin[1], Therese LaRue[3], Amanda Schrager-Lavelle[4], Cara H. Haney[5], Rita Nieu[6], Julin Maloof[4], John P. Vogel[7], José R. Dinneny[1, 12]

[1] Department of Plant Biology, Carnegie Institution for Science, Stanford, CA, USA.

[2] PhytoSystems, University of Liège, Liège, Belgium.

[3] Department of Biology, Stanford University, Stanford, CA, USA.

[4] Department of Plant Biology, UC Davis, Davis, CA, USA.

[5] Harvard Medical School, Massachusetts General Hospital, Department of Genetics, Department of Molecular Biology Boston, MA, USA

[6] USDA Western Regional Research Center, Albany, CA, USA

[7] DOE Joint Genome Institute, Walnut Creek, CA, USA

[8] These authors contributed equally

[9] Present address: Laboratorio Nacional de Genómica para la Biodiversidad (Langebio), Unidad de Genómica Avanzada, Centro de Investigación y de Estudios Avanzados del Instituto Politécnico Nacional (CINVESTAV-IPN), Irapuato, Guanajuato, México

[10] Present address: Boyce Thompson Institute for Plant Research/USDA, Ithaca, NY, USA.

[11] Present address: Energy Biosciences Institute, UC, Berkeley, CA, USA

[12] Corresponding author

Author contributions:

RR-A: Conception, design and development of the growth and imaging system and Arabidopsis transgenic lines; acquisition, analysis and interpretation of data; drafting and revising

the article.

GL: Development of the GLO-RIA image analysis plugin, analysis and interpretation of data, drafting and revising the article.

HL: Acquisition of data, development of the tomato growth and imaging setup.

P-LP: Acquisition of data, analysis and interpretation of data

JS: Development of Brachypodium transgenic lines, acquisition and analysis of Brachypodium, Arabidopsis and tomato data.

MCY: Development of Arabidopsis and Brachypodium transgenic lines.

YG: Development of Arabidopsis transgenic lines.

CT: Acquisition and analysis of the QPCR data

TL: Acquisition and analysis of the QPCR data

AS-L: Contributed the unpublished dual-color tomato line.

CH: Contributed the unpublished *Pseudomonas fluorescens* CH267-lux strain.

RN: Contribution to the development of the Brachypodium transgenic line.

JM: Contributed the unpublished dual-color tomato line.

JPV: Contribution to the development of the Brachypodium transgenic line.

JRD: Conception, design and development of the growth and imaging system and Arabidopsis transgenic lines; acquisition, analysis and interpretation of data; drafting and revising the article.

All authors read and approve the final version of the manuscript.

Abstract

Root systems develop different root types that individually sense cues from their local environment and integrate this information with systemic signals. This complex multi-

dimensional amalgam of inputs enables continuous adjustment of root growth rates, direction and metabolic activity that define a dynamic physical network. Current methods for analyzing root biology balance physiological relevance with imaging capability. To bridge this divide, we developed an integrated imaging system called Growth and Luminescence Observatory for Roots (GLO-Roots) that uses luminescence-based reporters to enable studies of root architecture and gene expression patterns in soil-grown, light-shielded roots. We have developed image analysis algorithms that allow the spatial integration of soil properties, gene expression and root system architecture traits. We propose GLO-Roots as a system that has great utility in presenting environmental stimuli to roots in ways that evoke natural adaptive responses and in providing tools for studying the multi-dimensional nature of such processes.

Introduction

Plant roots are three-dimensional assemblies of cells that coordinately monitor and acclimate to soil environmental change by altering physiological and developmental processes through cell-type and organ-specific regulatory mechanisms[1,2]. Soil comprises a complex distribution of particles of different size, composition and physical properties, airspaces, variation in nutrient availability and microbial diversity[3,4]. These physical, chemical and biological properties of soil can vary on spatial scales of meters to microns, and on temporal scales ranging from seasonal change to seconds. Root tips monitor this environment through locally and systemically acting sensory mechanisms[5,6].

The architecture of the root system determines the volume of soil where resources can be accessed by the plant (rhizosphere) and is under both environmental and genetic control. Plasticity in growth parameters allows the plant to adjust its form to suit a particular soil. Lateral roots, which usually make up the majority of the total root system, often grow at an angle divergent from the gravity vector. This gravity set-point angle (GSA) is controlled by auxin biosynthesis and signaling and can be regulated by developmental age and root type[7]. Recent cloning of the *DRO1* Quantitative Trait Locus (QTL) demonstrates that natural

genetic variation is a powerful tool for uncovering such control mechanisms[8].

Specific root ideotypes (idealized phenotypes) have been proposed to be optimal for acquisition of water and nitrogen, which are distinct from ideotypes for low phosphorus. Based on computational modeling and field studies, the "steep, deep and cheap" ideotype proposed by Lynch and colleagues may provide advantages to the plant for capturing water and elements like nitrogen that are water soluble and therefore tend to move in the soil column with water. This ideotype consists of highly gravitropic, vertically oriented roots that grow deep in the soil column and develop large amounts of aerenchyma, which reduces the overall metabolic cost of the root system[3]. Other nutrients, like phosphorus, which have limited water solubility and are tightly bound to organic matter, usually accumulate in the top layers of soil and favor roots systems that are more highly branched and shallow. The low-phosphorus ideotype effectively increases root exploration at the top layers of soil[3]. Modeling of root system variables shows that optimum architecture for nitrogen and phosphorus uptake are not the same[9] and suggests tradeoffs that may affect the evolution of root architecture as a population adapts to a particular environmental niche[10].

Clearly, understanding the architecture of root systems and how environmental conditions alter root developmental programs is important for understanding adaptive mechanisms of plants and for identifying the molecular-genetic basis for different response programs. In addition, roots systems have complexity beyond their architecture that needs to be incorporated into our understanding of plant-environment interactions. Primary and lateral roots exhibit different stress response programs in Arabidopsis[2,11] and may play specialized roles in water and nutrient uptake. Thus, it is important to develop methods that allow for a multidimensional characterization of the root system that includes growth, signaling, and interactions with other organisms. Furthermore, physiological parameters that affect whole plant responses to the environment, such as transpiration, are likely integrated into such processes, thus requiring a more holistic approach to studies of root function.

Based on these considerations we have developed a new root imaging platform, Growth and Luminescence Observatory for Roots (GLO-Roots), which allows root architecture and

gene expression to be studied in soil-grown plants. GLO-Roots is an integrated system composed of custom growth vessels, luminescent reporters and imaging systems. We use rhizotrons that have soil volumes equivalent to small pots and support growth of Arabidopsis from germination to senescence. To visualize roots, we designed plant-codon optimized luciferase reporters that emit light of different wavelengths. To visualize reporter expression, plants are watered with a dilute luciferin solution and imaged afterwards. We have built a custom luminescence imaging system that automatically captures images of rhizotrons held vertically. The signal from each reporter is distinguished using band-pass filters held in a motorized filter wheel, which enables automated acquisition of images from plants expressing both structural and environmentally and developmentally responsive reporters. We have also developed GLO-RIA (GLO-Roots Image Analysis), an ImageJ[12] plugin that allows for automated determination of (among other traits) root system area, convex hull, depth, width and directionality, which quantifies the angle of root segments with respect to gravity. GLO-RIA is also able to relate root system parameters to local root-associated variables such as reporter expression intensity and soil-moisture content.

Overall GLO-Roots has great utility in presenting environmental stimuli to roots in physiologically relevant ways and provides tools for characterizing responses to such stimuli at the molecular level in whole adult root systems over broad time scales.

Box 1.

All resources for GLO-Roots, including the original raw data used in the manuscript, sample images, GLO-RIA user manual, the latest software updates and the source code, can be found at: https://dinnenylab.wordpress.com/glo-roots/

Results.

We have developed an integrated platform for growing, imaging and analyzing root growth that provides advances in physiological relevance and retains the ability to visualize aspects

of root biology beyond structure.

The GLO-Roots platform.

GLO-Roots is comprised of four parts: i) growth vessels called rhizotrons that allow plant growth in soil and root imaging; ii) luminescent reporters that allow various aspects of root biology to be tracked in living plants; iii) GLO1 luminescence-imaging system designed to automatically image rhizotrons; iv) GLO-RIA, an image analysis suite designed to quantify root systems imaged using GLO-Roots.

Plant growth system. GLO-Roots utilizes custom designed growth vessels classically known as rhizotrons, which hold a thin volume of soil between two sheets of polycarbonate plastic. Acrylic spacers provide a 2-mm space in which standard peat-based potting mix is added. Black vinyl sheets protect roots from light and rubber U-channels clamp the rhizotron materials together. Plastic racks hold the rhizotrons vertically and further protect the roots from light. Rhizotrons and rack are placed in a black tub and water is added, to a depth of about 2 cm, at the bottom to maintain moisture in the rhizotrons during plant growth. The volume of soil in the rhizotrons (100 cm^3) is similar to small pots commonly used for Arabidopsis and supports growth throughout the entire life cycle (Fig 1A-C and Supplement 1).

To determine how the biology of plants grown in rhizotrons compares to other standard growth systems, we utilized high-throughput qRT-PCR to study how these conditions affect expression of 77 marker genes in root and shoot samples. These genes were curated from the literature and belong to a wide array of biological pathways including nutrient acquisition, hormone and light response and abiotic stress. Whole roots and shoot samples were collected at the end of the light and dark periods (Long-day conditions: 16 hour light, 8 hours dark) from plants grown in rhizotrons, pots, and petri dishes with two different media compositions: 1X Murashige and Skoog basal salts (ms) 1% sucrose or 0.25X ms, no sucrose (ms25). Principal component analysis of the gene expression values showed a separation of soil and gel-grown root systems in the the first principal components (Figure

1-figure supplement 1A). In roots grown on gel-based media, we observed enhanced expression of genes associated with light-regulated pathways (flavonoid biosynthesis: *FLAVINOL SYNTHASE1, FLS1*, *CHALCONE SYNTHASE, CHS* and photosynthesis: *RUBISCO SUBUNIT 1A, RBCS1A*, *CYCLOPHILIN 38, CYP38*), which is expected due to the exposure of gel-grown roots to light. In addition, genes associated with phosphorus nutrition (*LOW PHOSPHATE RESPONSE1*, *LPR1, PHOSPHATE STARVATION RESPONSE1, PHR1*) were (Figure 1-figure table supplement 1) less expressed in soil-grown roots, suggesting differences in nutrient availability between the different growth systems. Interestingly, shoot samples where not as clearly separated by growth media and, instead, time of day had a greater effect (Figure 1-Supplement 2). These data suggest root systems may be particularly sensitive to media conditions and indicate that rhizotron-grown root systems more closely approximate the biology of pot-grown plants than standard gel-based media. Shoot weight and primary root length were significantly reduced for gel-grown plants compared to rhizotron- or pot-grown plants suggesting significant differences in the biology of plants grown under these conditions (Figure 1-figure supplement 1B-C).

While the 2 mm depth of the soil sheet is 10 to 20 times the average diameter of an Arabidopsis root (between 100-200 microns[13]), we evaluated whether rhizotron-grown plants exhibited any obvious stress as a consequence of physical constriction. We compared traits of plants growing in vessels that hold similar volumes of soil but in different volumetric shapes. The number of lateral roots was significantly lower in pot and cylinder-grown plants compared to rhizotron-grown plants (Figure 1-figure supplement 1D) whereas primary root length of rhizotron and cylinder-grown plants was significantly greater than pot-grown plants (Figure 1-figure supplement 1E). No significant differences in shoot area were observed between the three systems (Figure 1-figure supplement 1-data). Thus, these data do not support the hypothesis that rhizotron-grown plants experience physical constriction greater than other vessels holding the same volume of soil.

Generation of transgenic plants expressing different luciferases. Arabidopsis roots cannot easily be distinguished from soil using brightfield imaging due to their thinness and

translucency (Figure 1-figure supplement 3); thus, reporter genes are needed to enhance the contrast between the root and their environment. Luciferase is an ideal reporter to visualize roots: 1) unlike fluorescent reporters, luciferase does not require high-intensity excitation light, which could influence root growth, 2) peat-based soil (a type of histosol) exhibits no autoluminescence but does autofluoresce at certain excitation wavelengths similar to GFP (Figure 1-figure supplement 3), 3) while GFP is very stable, and thus not as suitable for imaging dynamic transcriptional events, the luciferase enzyme is inactivated after catabolism of luciferin, making it ideal for studying processes such as environmental responses. A considerable number of luciferases have been developed that emit light spanning different regions of the visible spectrum, but their utilization has been limited to studies in animals (Table 1).

Table 1: Luciferases used in this study.

Luciferase	Origin	maximum wavelength	Substrate
Ppy RE8	firefly	618	D-luciferin
CBGRed	click beetle	615	D-luciferin
venus-LUC2	FP + firefly	580	D-luciferin
LUC(+)	firefly	578	D-luciferin
CBG99	click beetle	537	D-luciferin
lux operon	A. fischeri	490	biosynthesis pathway encoded within operon
nanoLUC	Deep sea shrimp	470	furimazine

To determine the efficacy of using luciferase to visualize roots in soil, we codon optimized sequences of *PpyRE8*, *CBGRed*, *LUC2*, and *CBG99* for Arabidopsis expression. In addition, nanoLUC[14] and venus-LUC2[15] were utilized. Constitutive luciferase expression was driven in plants using the *UBIQUITIN 10 (UBQ10)* or *ACTIN2 (ACT2)* promoters using vectors assembled through a Golden-Gate cloning system[16]. Plants homozygous for a single locus T-DNA insertion were evaluated for in vivo emission spectra and luminescence intensity (Fig 1D). All the evaluated luciferases use D-luciferin as a substrate facilitating the simulta-

neous imaging of different luciferases except nanoLUC, which uses a proprietary substrate furimazine[14]. Luciferases with red-shifted emission spectra were less intense than the green-shifted luciferases (Fig 1D). LUC2o showed an emission maximum at 580 nm and a minor peak at 620 nm while CBG99o lacks the minor peak.

Continuous addition of luciferin did not have any significant effect on shoot weight or primary root length (Figure 1-figure supplement 4). After luciferin addition, luminescence signal could be reliably detected in root systems for up to 10 days, depending on the developmental state of the plant.

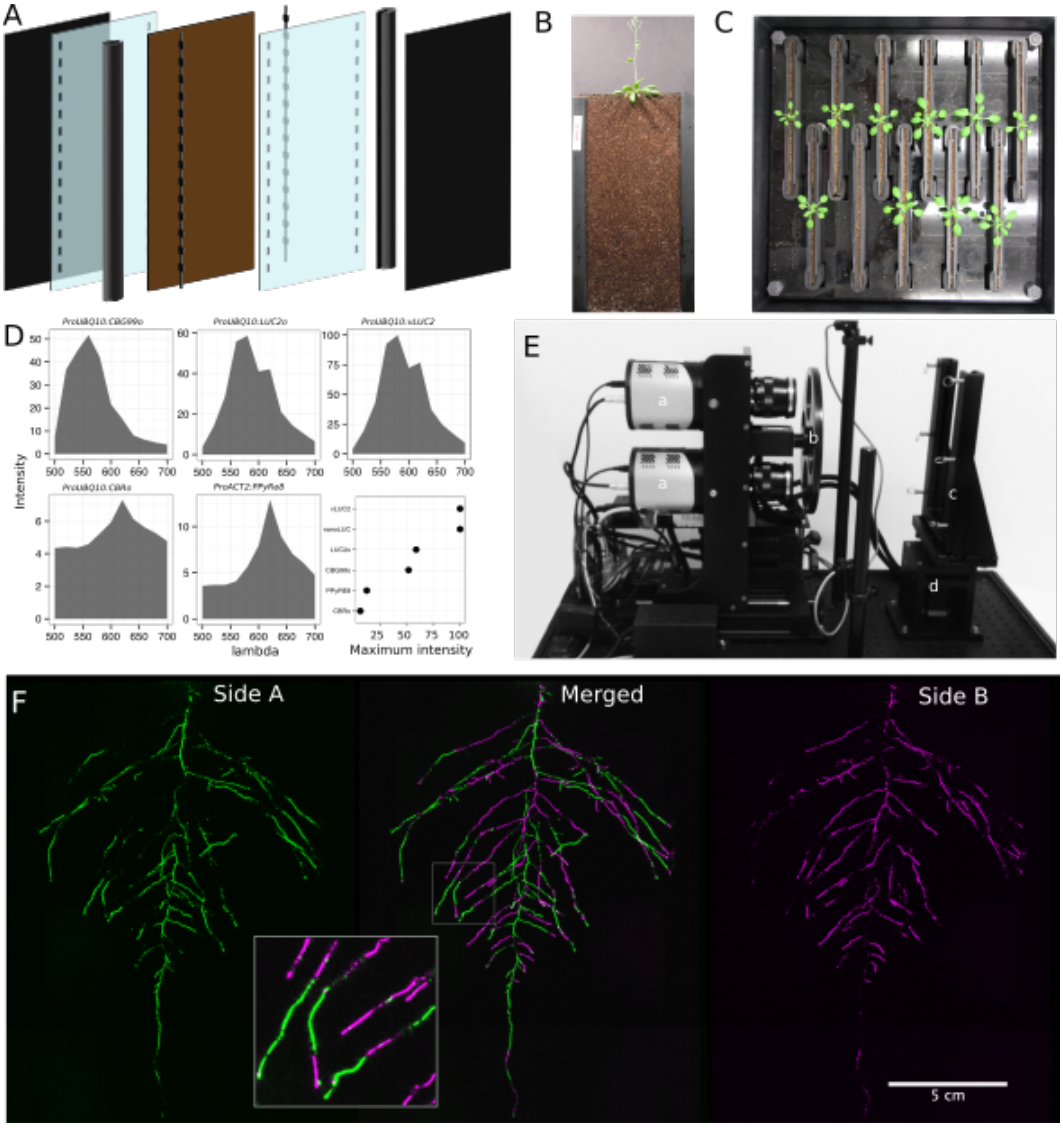

Figure 1. GLO-Roots growth and imaging systems A) 3D representation of the different physical components of the rhizotron: plastic covers, polycarbonate sheets, spacers and rubber U-channels. Blueprints are provided in Supplementary material 1. In brown, soil layer. B) Thirty five day-old plant in rhizotron with black covers removed. C) Top view of holding box with eleven rhizotrons. D)In vivo emission spectra of different luciferases used in this study. Transgenic homozygous lines expressing the indicated transgenes were grown on agar media for 8 days. Luciferin (300 µM) was sprayed on the seedlings and

plates were kept in the dark and then imaged for 2 s at wavelengths ranging from 500 to 700 nm. Five intensity values were taken from different parts of the roots of different seedlings and averaged. Relative maximum intensity values are indicated in the lower right graph. E) GLO 1 imaging system. The system is composed by two back illuminated CCD cameras (a) cooled down to -55 ^{o}C. A filter wheel (b) allows for spectral separation of the different luciferases. On the right, a rhizotron holder (c) is used to position the rhizotrons in front of the cameras. A stepper motor (d) rotates the rhizotron 180^{o} to image both sides. F) A 21 DAS plant expressing *ProUBQ10:LUC2o* was imaged on each of two sides of the rhizotron; luminescence signal is colorized in green or magenta to indicate side. In the middle of the panel, a combined image of the two sides is shown. The inset shows a magnified part of the root system. FW: fresh weight, PR: Primary root.

GLO1: a semi-automated luminescence imaging system for rhizotrons. Luminescence imaging systems commercially available for biomedical research are usually optimized for imaging horizontally held specimens or samples in microtiter plates. Placing rhizotrons in this position would induce a gravitropic response in plants. Working with Bioimaging Solutions (San Diego, CA) we designed and built a luminescence imaging system optimized for rhizotron-grown plants. GLO1 (Growth and Luminescence Observatory 1) uses two PIXIS-XB back-thinned CCD cameras (Princeton Instruments, Trenton, NJ, USA) to capture partially-overlapping images of rhizotrons while a motorized stage automatically rotates the rhizotron to capture images of both sides (Fig 1E). A composite image is generated from the images captured of each side; Fig 1F shows that approximately half of the root system is revealed on each side with few roots being visible on both sides. Apparently, the soil sheet is thick enough to block portions of the root system but thin enough to ensure its continuous structure can be compiled from opposite face views. We tested the ability of GLO1-generated images to reveal complete root systems by manually quantifying the number of lateral roots in excavated root systems of 8 different plants and testing these results against estimates of lateral root number from images of the same plants visually inspected by 4 different persons. These comparisons revealed good correlation ((R^2= 0.974))

between actual lateral root counts and image-based estimation, indicating GLO1-generated root images provide an accurate representation of the in soil root system.

GLO-RIA: GLO-Roots Image Analysis. We developed a set of image analysis algorithms that were well suited for the complex root systems that GLO-Roots is able to capture. GLO-RIA (Growth and Luminescence Observatory Root Image Analysis) is an ImageJ plugin divided in two modules.

The first module (RootSystem) performs four different types of analysis: i) a local analysis that detects all root particles in the image and computes their position, length and direction; ii) the global analysis performs a root system level analysis and computes the total visible surface, convex hull, width and depth; iii) the shape analysis uses Elliptic Fourier Descriptors or pseudo-landmarks similarly to RootScape[17] to perform a shape analysis on the root system iv) the directionality analysis computes the mean direction of root particles in a root system (either on the full image or by a user-defined region of interest in the image). These four analysis methods are fully automated by default, but can be manually adjusted if needed.

The second module of GLO-RIA (RootReporter) was specifically designed for the analysis of multi-layered images such as combinations of gene reporter, root structure and soil moisture. Shortly, the plugin works as follows: i) detection of the gene reporters and the structure reporters in their respective images; ii) if needed, a manual correction can be performed to correct the automated detection; iii) gene reporters are linked with the soil water content and the structure reporters, based on their proximity; iv) gene reporter intensity (either absolute or normalized using the structural reporter) is computed; v) all data are exported and saved to a Root System Markup Language (RSML) datafile[18]. Gene and structure reporters can be followed across different time and space points. Using an object oriented approach, great care has been taken to facilitate the user interactions on the different images to streamline the analysis process. Table 2 shows a list of root system features extracted using GLO-RIA.

Table 2: list of root system features extracted using GLO-RIA.

variable	unit
projected area	cmˆ2
number of visible roots	-
depth	cm
width	cm
convex hull area	cmˆ2
width	cm
feret	cm
feret angle	°
circularity	-
roundness	-
solidity	-
center of mass	cm
Directionality	°
Euclidean Fourier Descriptors	-
Pseudo landmarks	-

GLO-RIA does not currently have the ability to reconstruct the root architecture in itself (topological links between roots). This is a challenge for analyzing images captured by GLO-Roots since soil particles cause disruption of root segments.

We tested the accuracy of the measurements obtained from GLO-RIA using two different ground-truthed data sets. Manual measurement of root system width, depth and average lateral root angle was determined by hand using imageJ from an independent set of images corresponding to roots of several Arabidopsis accessions growing in control conditions. We also used ArchiSimple[19] to generate 1240 images of root system models with contrasting sizes and lateral root angles. Since these images are computationally generated, exact determination of root system parameters was possible. For both ground truth data sets, GLO-RIA quantification provided measurements that were well correlated for all all three measured

parameters (Figure 1-figure supplement 5D-F). Sample images of real and ArchiSimple generated root images are shown with GLO-RIA-defined directionality color-coding (Figure 1-figure supplement 5G-I).

Continuous imaging of root growth.

The size of our rhizotrons enables undisturbed root system development (before roots reach the sides or the bottom of the rhizotron) for about 21-23 days for the Col-0 accession growing under long day conditions (Figure 2); however root traits such as directionality can be observed through later stages of plant development. See 35 DAS root system and directionality in Figure 2A-B. An example of a time series spanning 11 to 21 days after sowing (DAS) of Col-0 roots expressing *ProUBQ10:LUC2o* is shown in Fig 2A and Video 1 with a color-coded time projection shown in Fig 2C. Directionality analysis (Fig 2B) shows a progressive change in root system angles from 0^{o} (vertical) to 45^{o} as lateral roots take over as the predominant root type. Figure 2D shows the evolution over time of several root traits that can be automatically captured by GLO-RIA (depth, width, area) and others that were manually quantified (primary root growth rate or number of lateral roots per primary root).

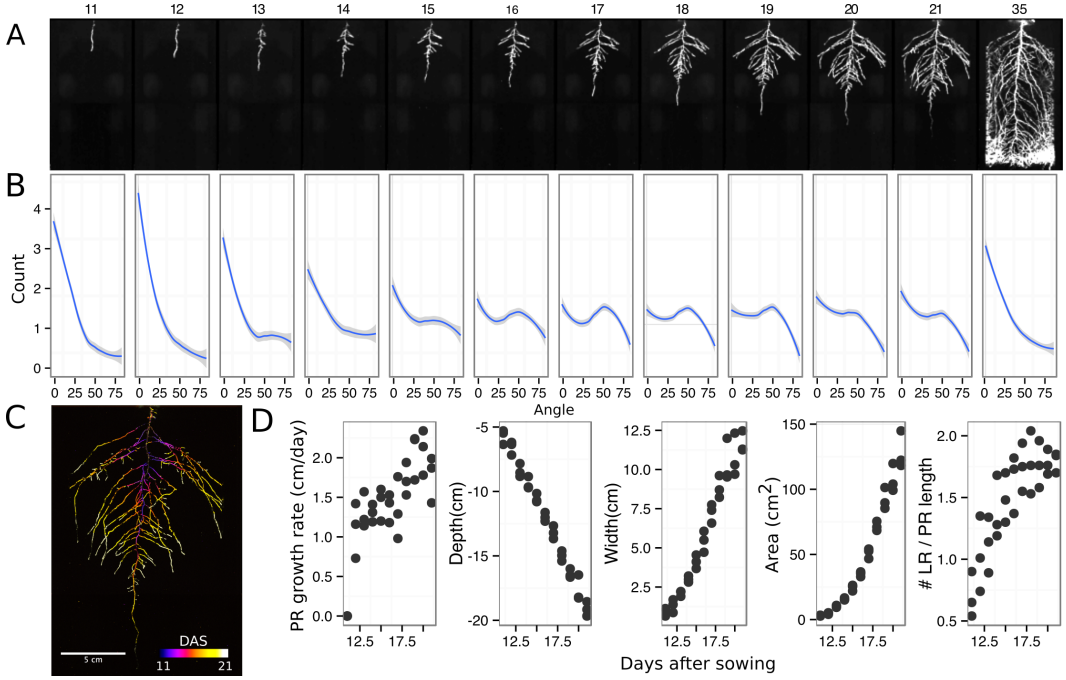

Figure 2. Time-lapse imaging of root systems and quantification using GLO-RIA. A) Typical daily time-lapse image series from 11 to 35 DAS of a *ProUBQ10:LUC2o* Col-0 plant. B) Directionality of the root system of plants in panel A calculated using the directionality plugin implemented in GLO-RIA. C) Color coded projection of root growth using the images in panel A. D) Primary root growth rate, depth, width, root system area are automatically calculated from the convex hull, which is semi-automatically determined with GLO-RIA. Lateral root number and number of lateral roots divided by the primary root length were quantified manually. A Local Polynomial Regression Fitting with 95% confidence interval (grey) was used to represent the directionality distribution curve. (0^o is the direction of the gravity vector).

Root system architecture of different Arabidopsis accessions.

As a proof of concept to estimate the utility of our root imaging system to phenotype adult root system traits, we transformed a small set of accessions (Bay-0, Col-0 and Sha) with the *ProUBQ10:LUC2o* reporter and quantified RSA at 22 DAS (Fig 3A-C). GLO-RIA

316 analysis of these root systems identified several root traits that distinguish Col-0, Bay-0
317 and Sha. Directionality analysis revealed an abundance of steep-angle regions in the root
318 system of Bay while Sha showed an abundance of shallow-angled regions and Col-0 was
319 intermediate (Fig 3D). Bay-0 shows the deepest and narrowest root system leading to the
320 highest depth/width ratio while Sha has the widest root system (Fig 3E). Other root traits
321 such as root system area and the vertical center of mass also showed significant differences
322 (Figure 3-figure supplement 1B). Broad sense heritability values for depth (96.3), area (92.0),
323 depth/width (97.8), width (95.7) and vertical center of mass (95.0) were all higher than 90%.
324 To capture the richness of root architecture shape, we used GLO-RIA to extract pseudo-
325 landmarks describing the shape of the root system (see Materials and Methods for more
326 details) and performed PCA analysis. The first principal component captures differences
327 in the distribution of widths along the vertical axis and separates Col-0 and Sha from Bay-
328 0 root systems. (Fig 3F). Bay-0 shows an homogenous distribution of widths along the
329 vertical axis while Sha and Col-0 are much wider at the top than bottom. PC2 seems to be
330 capturing a relationship between width at the top and total depth and separates Sha root
331 systems which are wide at the top and deep from Col-0 root systems which are wide but
332 not as deep as Sha. Shape information extracted from pseudo-landmarks can distinguish
333 the three different accession using PCA analysis (Fig 3G).

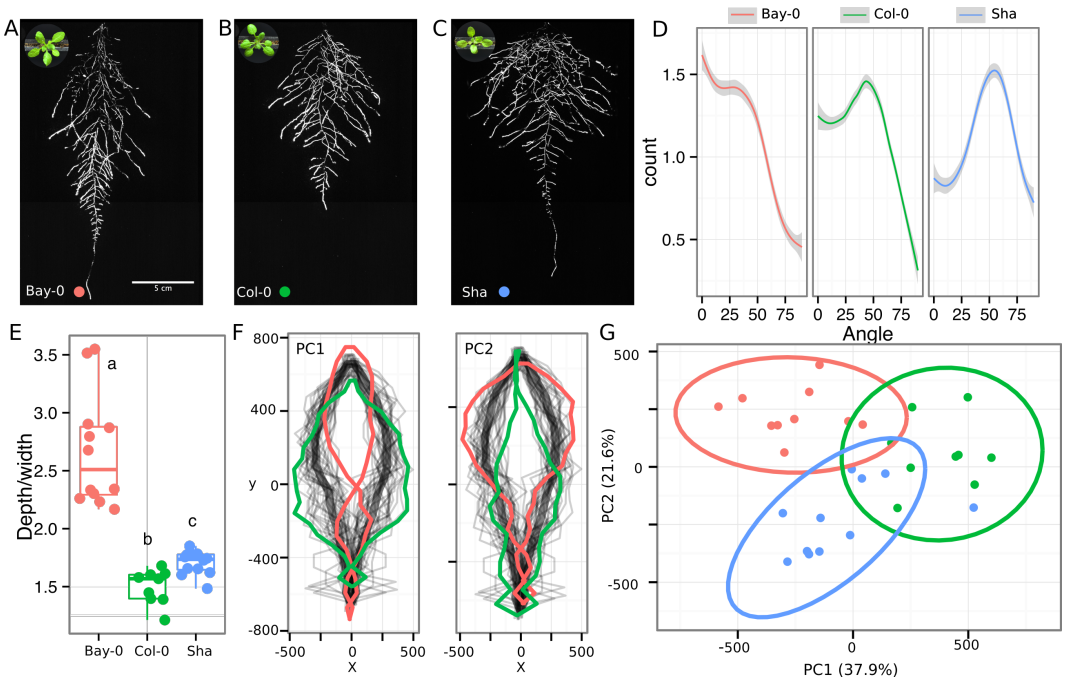

Figure 3. Variation in root architecture between accessions of Arabidopsis. Representative root and shoot images of A) Bay-0, B) Col-0 and C) Sha accessions transformed with _ProUBQ10:LUC2o_and imaged after 22 DAS. D) Directionality of the root systems, E) depth/width ratio, F) Pseudo-landmarks describing shape variation in root system architecture. Eigenvalues derived from the analysis of 9-12 plants per accession is shown. The first two Principal Components explaining 38% (PC1) and 22% (PC2) of the shape variation are plotted. PC1 captures homogeneity of root system width along the vertical axis and PC2 a combination of depth and width in top parts of the root system. Red and green lines indicate -3SD and +3SD (Standard Deviations), respectively G) PC separation of the different ecotypes using the PCs described in (F). A Local Polynomial Regression Fitting with 95% confidence interval (grey) was used to represent the directionality distribution curve. 0^{o} is the direction of the gravity vector. Wilcoxon test analysis with $p < 0.01$ was used to test significant differences between the different accession (n = 9-12 plants).

Spectrally distinct luciferases enable gene expression patterns, characterization of root system interactions and microbial colonization.

We tested whether spectrally distinct luciferase reporters would enable additional information besides root architecture to be captured from root systems. Luciferase reporters have been commonly used to study gene expression and these resources can potentially be utilized to study such regulatory events in soil-grown roots. We transformed *ProACT2:PpyRE8o* into two well studied LUC reporter lines: the auxin response reporter line *ProDR5:LUC+*[20] (Figure A-B) and the Reactive Oxygen Species (ROS) response reporter *ProZAT12:LUC*[21] (Figure 4C-D). We implemented in GLO-RIA an algorithm that semi-automatically identifies gene reporter signal and associates this object to the corresponding root structure segment. A graphical representation of the results obtained with Root Reporter can be observed in Figure 4-figure supplement 1. Reporter intensity values along the first 5 mm of root tips can also be observed in Figure 4-figure supplement 2.

We then took advantage of our ability to constitutively express two spectrally different luciferases and imaged the overlapping root systems (one expressing *ProUBQ10:LUC2o* and the other *ProACT2:PPy RE8o*). While two root systems were distinguishable using this system (Figure 4-figure supplement 3); measurements of root system area did not reveal a significant effect on root growth when two plants were grown in the same rhizotron, compared to one; however, further studies are warranted (Figure 4-figure supplement 3).

The GLO-Roots system uses non-sterile growth conditions, which allows complex biotic interactions that may affect responses to the environment. Bacteria themselves can be engineered to express luminescent reporters through integration of the LUX operon, which results in luminescence in the blue region of the spectrum and is thus compatible with the plant-expressed luciferase isoforms we have tested. *Pseudomonas fluorescens* CH267[22], a natural Arabidopsis root commensal, was transformed with the bacterial LUX operon and used to inoculate plants. Thirteen days after inoculation, we were able to observe bacterial luminescence colocalizing with plant roots. *P. fluorescens* did not show an obvious pattern of colonization at the root system scale level. As a proof-of-principle test

of the multi-dimensional capabilities of the GLO-Roots system we visualized both *LUC2o* and *PPyRE8o* reporters in plants and the LUX reporter in bacteria in the same rhizotron (Figure 4-figure supplement 4).

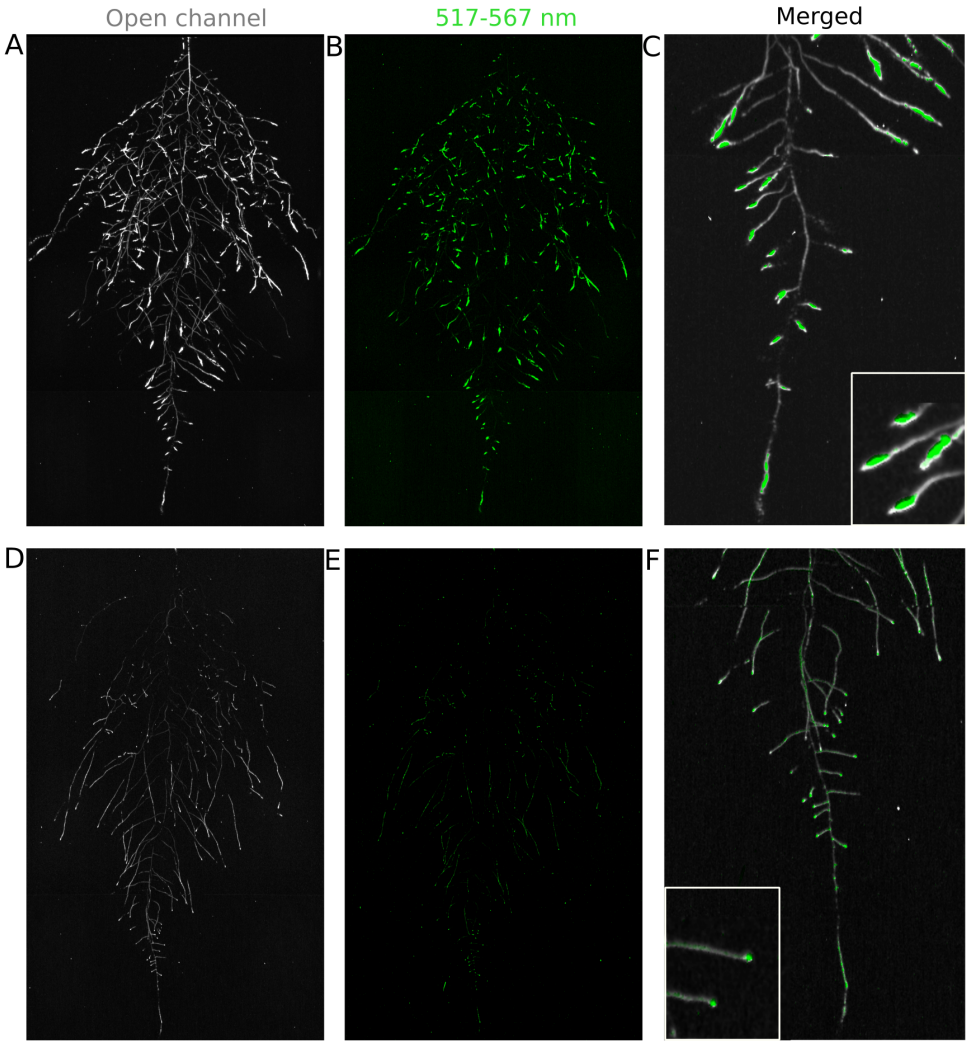

Figure 4. Dual-color reporter visualization of structure and gene expression. Images of whole root systems (A, D) or magnified portion of roots (C, F) at 22 DAS expressing *ProDR5rev:LUC+* (green, A, B) or *ProZAT12:LUC* signal (green, D, E)with skeletonized representation of roots generated using the *ProACT2:PpyRE8o* reporter expression (in grey).

Adaptive changes in root system architecture under water deprivation, phosphorus deficiency and light. To test the utility of the GLO-Roots system to understand response of root systems to environmental stimuli we tested the effects of light and conditions that mimic drought and nutritional deficiency. To examine the effects of light exposure on the root architecture, the black shields, which normally protect the soil and roots from light, were removed from the top half of the rhizotrons 10 DAS. Using directionality analysis we detected a significant increase in the steepness of roots only in the light exposed region of the rhizotron, while the lower shielded region showed no difference. (Fig 6-figure supplement 3A-B and Fig 6-figure supplement 4). Light can penetrate the top layers of soil[23] and it has been proposed to have a role in directing root growth specially in dry soils[24] through the blue light receptor *phot1*. Root directionality was not significantly different between light and dark-treated roots of the *phot1/2* double mutant suggesting that blue light perception is necessary for this response[24,25] (Fig 6-figure supplement 3B-lower panel). These data highlight the strong effects of light on root system architecture[26], which GLO-Roots rhizotrons are able to mitigate.

Plants grown in low-P soil showed a significant increase in the width-depth ratio of the root system compared to plants grown in P-replete soil, as determined using the automated root system area finder in GLO-RIA (Fig 6-figure supplement 2A-B). Plants under P deficiency showed an increase in the ratio between root-shoot area (Fig 6-figure supplement 2C) and higher investment of resources in the development of the root system at the expense of shoot growth (Fig 6-figure supplement 2D). Root systems of control and P-deficient plants showed no significant differences in directionality at 22 DAS but at 27 DAS, roots were more horizontally oriented in P-deficient plants (Fig 6-figure supplement 2E). The observed changes in root architecture are consistent with root system ideotypes that improve phosphorus uptake efficiency.

GLO-Roots is especially well suited for studying water-deficit (WD) responses. First, shoots are exposed to the atmosphere and vapor pressure deficit is maintained at levels that allow for transpiration of water from the shoot. Second, soil in rhizotrons is exposed to air at

the top and dries from the top-down; drying soil increases the volume occupied by air and reduces contact of root with liquid water, all of which are similar to changes in soil expected in the field during WD. Finally, as peat-based soil dries, its optical properties change, allowing moisture content to be approximated from bright-field images. We took advantage of the change in gray-scale pixel intensity to construct a calibration curve (Figure 5-figure supplement 1) that quantitatively relates gray-scale pixel intensity to moisture content (Fig 5A); water content can be color coded in images with appropriate look up tables (Fig 5B). Soil color was not affected by the presence or absence of roots (Figure 5-figure supplement 2). Using this approach, water content in a rhizotron can be mapped and visualized in 2D (Fig 5C-D). In the example shown, we can observe that a 22 DAS Bay-0 plant depleted soil-moisture content locally around the root system (Figure 5E).

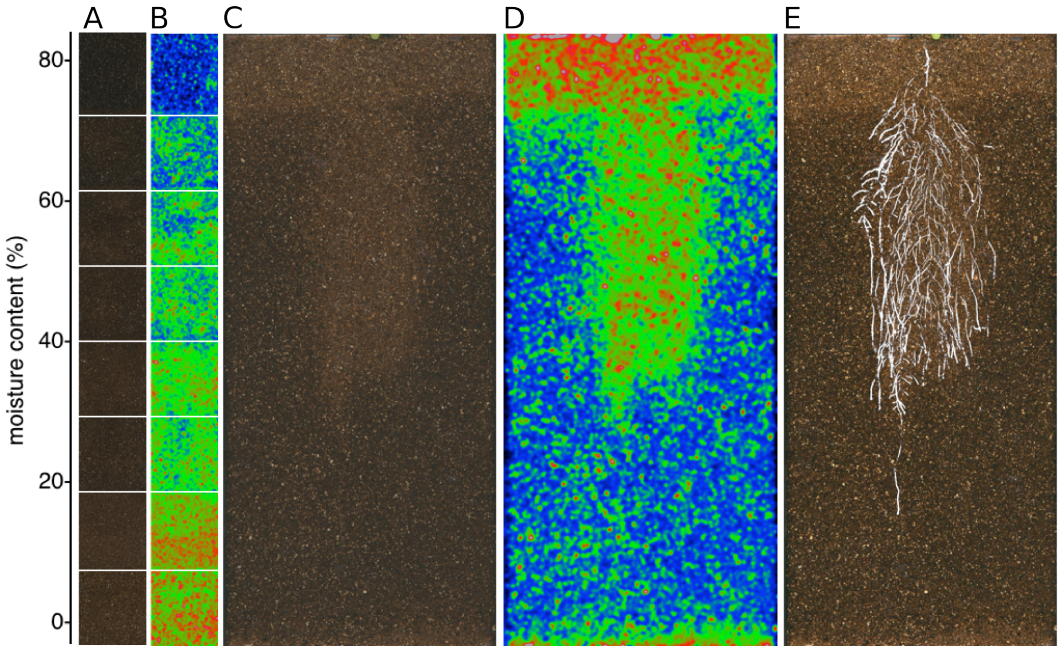

Figure 5. Soil moisture and root architecture mapping in rhizotrons. A) Composite image showing regions of soil made from rhizotrons prepared with different moisture levels. B) Differences in grey-scale intensity values were enhanced using a 16-color Look Up Table (LUT). Brightfield image of soil in rhizotron (C) and converted using 16-color LUT to enhance visualization of distribution of moisture (D) . E) Root system of a Bay-0

22 DAS and subjected to water deprivation since 13 DAS. Root system visualized using luminescence and overlaid on brightfield image of soil in (C).

We performed several trials to simulate WD in our growth system. Plants were germinated, grown under control conditions then transferred to 29ºC and standing water removed from the container holding the rhizotrons starting at 9 DAS or 13 DAS. Elevated temperature combined with water deficit is a common stress that modern crops varieties are poorly adapted to, thus highlighting the importance of examining this combined treatment[27,28]. Plants were maintained in this WD regime until 22 DAS when luciferin solution was added and the plants imaged. At 13 DAS, lateral roots near the soil surface are already emerged (Video 1, Figure 2A) and 9 days of subsequent WD treatment caused lateral roots to show an increase in gravitropism leading to the development of a root system that were deeper and more vertically oriented (Fig 6A). Roots of Bay-0 plants showed similar responses, though the extent of change was less pronounced since Bay-0 roots are normally more vertically oriented (Fig 6B). Plants transferred at 9 DAS and grown for 13 days under WD showed less lateral root development in the top layer of soil (Fig 6E). At this time point, lateral roots start to emerge (Video 1) and early drought may lead to growth quiescence or senescence. Careful examination of roots in these regions showed evidence of small lateral root primordia populating the primary root (Figure 6F). After 24 h of re-watering (Figure 6G) these lateral root primordia reinitiated growth (Figure 6H).

Time-lapse imaging of the water deficit response showed that changes in root growth direction occurred ahead of the dry soil front Video 2. Using GLO-RIA we were able correlate local water moisture contents with the orientation of root segments. With this approach we observed that root segments in dryer areas of rhizotron grew at steeper root angles (Figure 7) than roots in WW regions, though lateral root angle in wetter regions was also affected. These data suggest that both local and systemic signaling is likely involved in redirecting lateral roots deeper during the simulated drought treatments tested here.

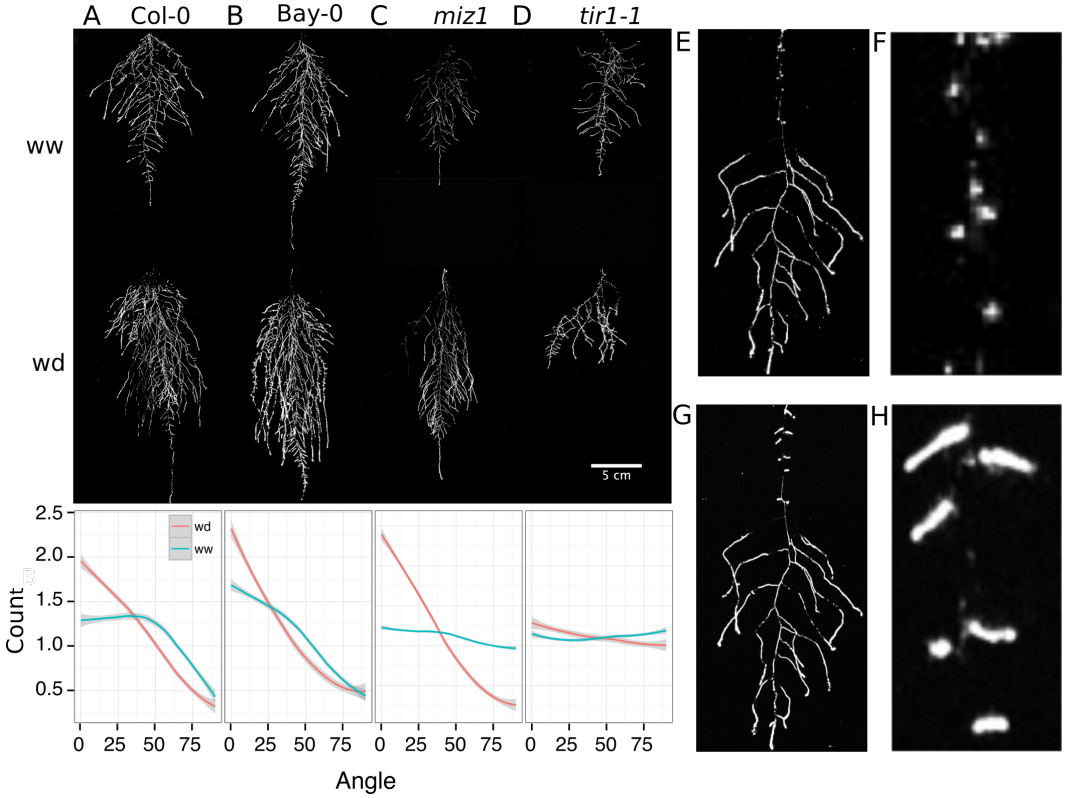

Figure 6. Study of effect of water deficit on root system architecture. A-D) Root systems 22 DAS and exposed to water deficit 13 DAS onwards. Sample images of well watered (left panels) and water deficit (right panels) root systems treated from 13 DAS and directionality (line graphs to left of images) for (A) Col-0 (B) Bay-0 (C) *miz1* mutant and (D) *tir1-1* . E) Root system of a 22 DAS plant exposed to water deprivation from 9 DAS onwards with magnified view of lateral root primordia (F). G) The same root as in (E) 24 hours after rewatering and magnified view of lateral root primordia (H). Kolmogorov-Smirnov test at $p < 0.001$ was used to compare directionality distributions between the different treatments and genotypes. A Local Polynomial Regression Fitting with 95% confidence interval (grey) was used to represent the directionality distribution curve. 0^o is the direction of the gravity vector.

We also grew plants under WD at control temperatures or under WW conditions at elevated temperature to test the effects of these individual stresses on root architecture. We observed

that both conditions were sufficient to induce a change in root directionality indicating that the plant uses similar mechanisms to avoid heat and water-deficit associated stresses (Figure 6-figure supplement 1). We next asked which regulatory pathways controlled the observed changes in lateral root directionality during simulated drought. Hydrotropism is a known environmental response that directs root growth towards wet regions of soil. MIZ1 is an essential regulator of hydrotropism; however *miz1* mutants had no significant effect on water deficit-induced changes in root directionality, compared to wild type (Fig 6C), indicating that this response was distinct from hydrotropism. Auxin is an important mediator of gravitropism and auxin treatment causes lateral roots to grow more vertically[7]. Consistent with this role for auxin, mutant plants with loss of function in the auxin receptor TIR1, did not show changes in the root system directionality between WW and WD conditions (Fig 6D).

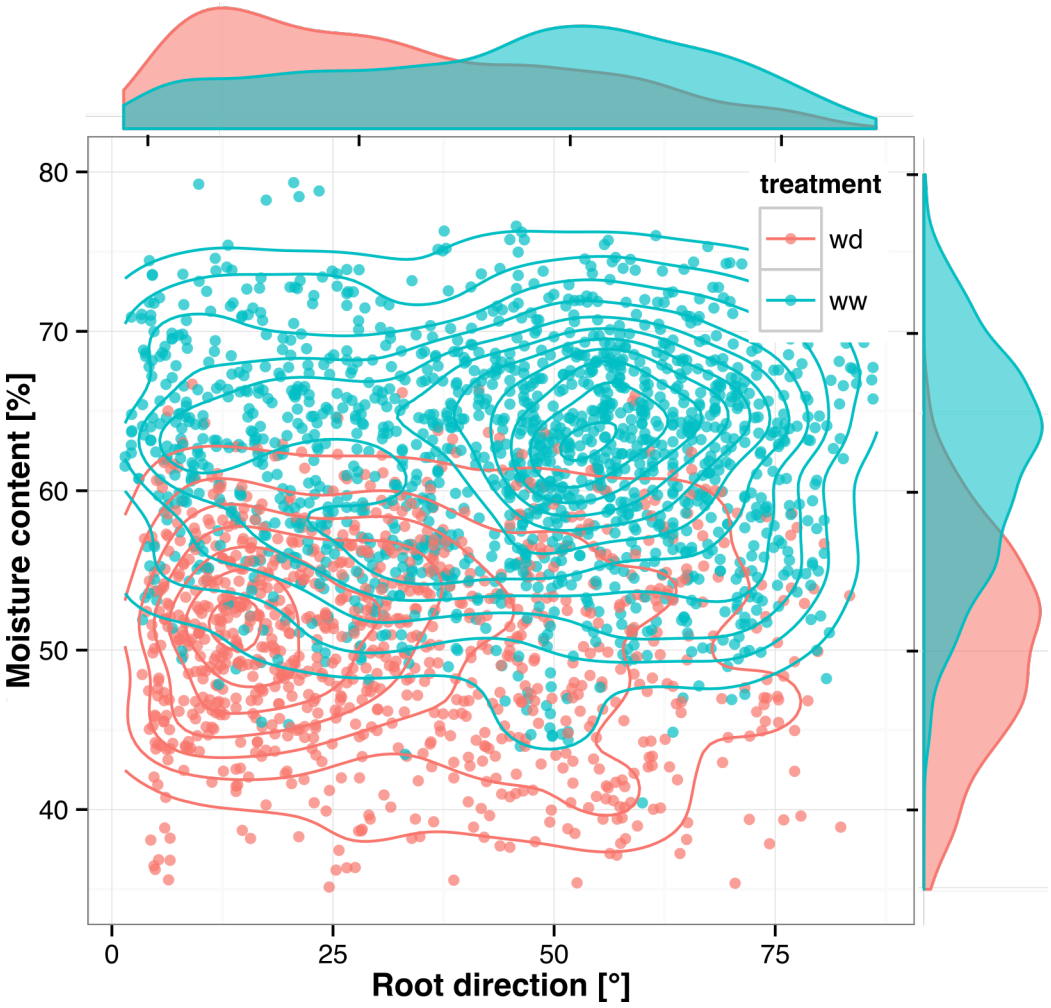

Figure 7. Relationship between local soil moisture content and root growth direction. Data quantified from the time lapse series shown in Video 2. Density plots shown at periphery of graph for root direction (x-axis) and soil moisture (y-axis). 0º is the direction of the gravity vector. Data represents 2535 root tips measured in a series encompassing 10 time points.

GLO-Roots for Brachypodium and Tomato.

To examine the general applicability of the GLO-Roots system for other species, we introduced LUC2o-expressing reporters into the model grass *Brachypodium distachyon* and the

crop plant *Lycopersicon esculentum* (tomato). Brachypodium is well suited to the GLO-Root system because, like Arabidopsis, its small size allows mature root systems to be studied in relatively small soil volumes[29,30]. *LUC2o* driven by the *ZmUb1* promoter was introduced into Brachypodium using the pANIC vector[31]. Brachypodium roots showed a distinct architecture from Arabidopsis marked by prolific development of secondary and tertiary lateral roots (Fig 8A). This is consistent with other studies that show that Brachypodium has a typical grass root system[30]. Comparison of root system development in rhizotrons with gel-based media showed that root growth is higher in soil than in plates (Figure 8-figure supplement 1). Previous work has suggested that auxin levels in Brachypodium roots is sub-optimal for growth[32]. Pacheco-Villalobos and colleagues suggest that, in Brachypodium, and contrary to what happens in Arabidopsis, ethylene represses *YUCCA* reducing the synthesis of auxin. The reduced growth that we observe in plates and the high levels of ethylene that build up in sealed plates[33] would support this mechanism.

Tomato plants were transformed with *Pro35S:PPyRE8o* and *ProeDR5rev:LUC2* reporters. The plants showed more rapid growth than Arabidopsis or Brachypodium and required fertilizer to prevent obvious signs of stress (reduced growth, anthocyanin accumulation). Root systems were imaged from 17 DAS plants. Roots showed presumptive lateral root primordia marked by DR5-expression (Fig 8C-D). These results show that the GLO-Roots method can be applied to study root systems of plants and will likely be useful for studying root systems of other small to medium sized model plants and for early stages of larger crop plants.

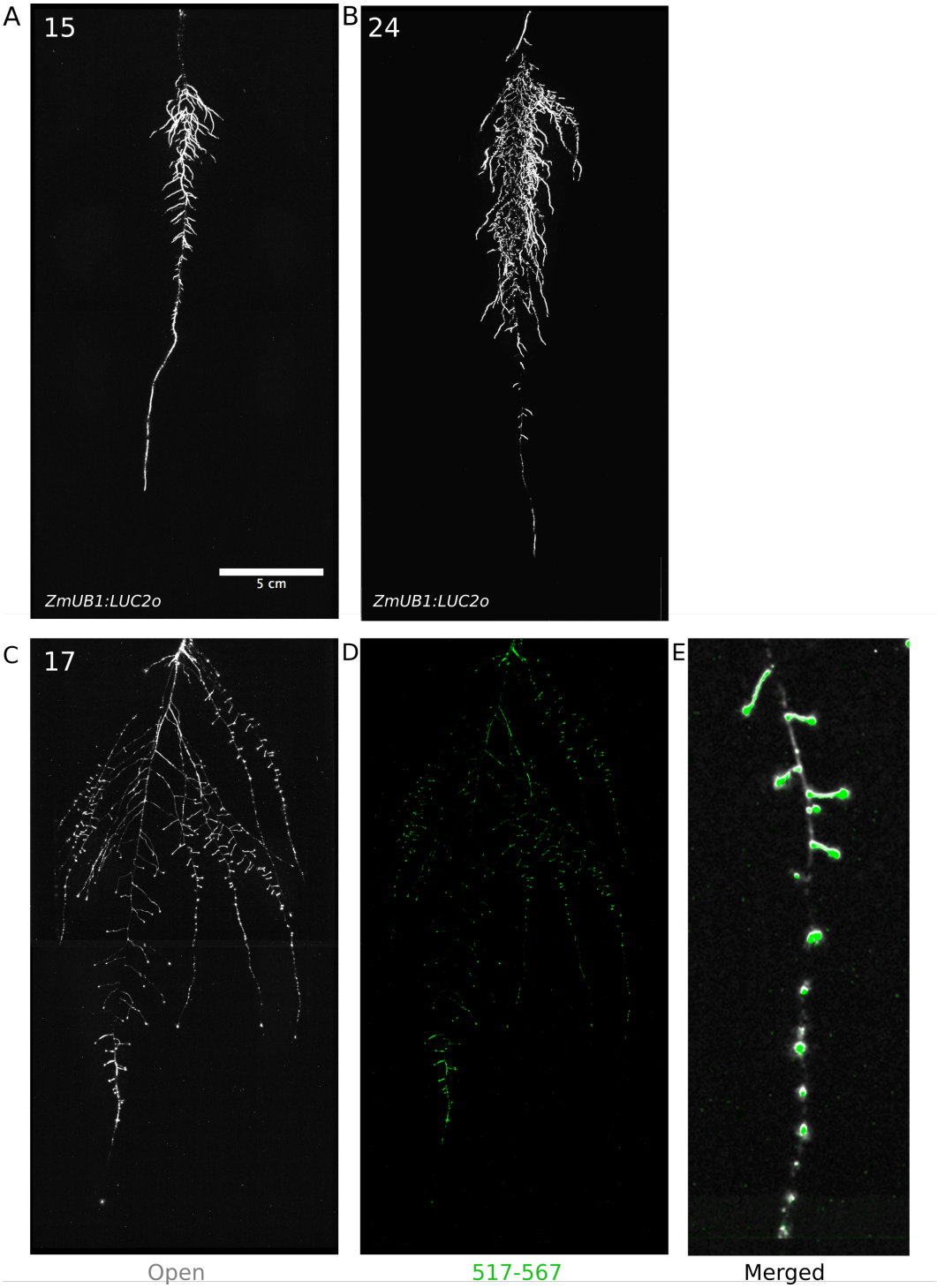

Figure 8: Roots of *Brachypodium distachyon* transformed with *ProZmUB1:LUC2o* and

514 imaged at 15 (A) and 24 (B) DAS grown in control conditions. C) Open channel of 17
515 DAS tomato plant transformed with *ProeDR5rev:LUC2o* and *Pro35S:PPyRE8o* D) Green
516 channel showing only *ProeDR5rev:LUC2o* E) Amplification of the open and green channel
517 showing increased expression of *ProeDR5rev:LUC2o* reporter in early-stage lateral roots.

518 ## Discussion.

519 ### GLO-Roots enables a multi-dimensional understanding of root biology.

520 Recent studies of root systems has emphasized structural attributes as important contrib-
521 utors of root system function. Indeed, studies examining the role of genetic variants in
522 tolerating abiotic stress have demonstrated the importance of such characteristics[8]. Roots,
523 however, are highly diverse in the biology they perform and a multi-dimensional understand-
524 ing of root systems, which incorporates differences in signaling, metabolism and microbial
525 association as well as structure, may provide a clearer understanding of the degree to which
526 sub-functionalization of the root system plays a role in important processes such as acclima-
527 tion and efficient resource acquisition.

528 We have developed tools in GLO-Roots that allow for tracking multiple aspects of soil
529 physicochemical properties and root biology simultaneously. Using GLO-Roots, we are able
530 to map in 2D coordinates soil physical properties such soil moisture together with root ar-
531 chitecture traits such as directionality, growth rates and gene expression levels. All this
532 information is aggregated in layers for each x, y coordinate. Using GLO-RIA we integrate
533 this multilayer information, leveraging our ability to simultaneously and seamlessly investi-
534 gate root responses to environmental stimuli such as soil moisture content. Luciferases that
535 emit light at different wavelengths allow for constitutive and regulated promoters to be stud-
536 ied together. Introduction of luciferase reporters into microbes provides an additional layer
537 of information that provides a readout on the association between organisms and how this
538 might be affected by environmental conditions. The flexibility of the GLO-Roots system may
539 enable additional dimensionality to our understanding of root biology. Other physical prop-

erties such as CO_2 or pH mapping in rhizotrons have already been enabled by using planar optodes[34]. It may be possible to engineer LUX-based reporters in microbes that are responsive to extracellular metabolites, creating microbial biosensors, and integration of such tools may enable root-exudation and nutrition to be analyzed in soil. Split-Luciferase reporters have been engineered that allow bi-molecular interactions to be studied. Finally, molecular sensors analogous to FRET sensors, termed BRET-sensors[35], may allow metabolite tracking dynamically through the root system. With additional innovation in the development of luciferase reporters, the GLO-Roots systems will likely expand the repertoire of biological processes that can be studied over an expanded range of developmental time points and environmental conditions.

Enhanced root growth and gravitropism may constitute an avoidance mechanism used during water deficit stress.

It has been proposed that plants with steep root systems will be better able to tap into deep water resources and thus perform better under water deprivation. For example in rice, the IR64 paddy cultivar shows shallow root systems in upland fields whereas Kinandang Patong, an upland cultivar, is deeper rooting[8]. Plants maintain a number of regulatory pathways that mediate changes in physiology during WD. Enhanced growth of root systems has been well characterized in field-grown plants; however this has not been recapitulated in studies of gel-grown Arabidopsis plants. Thus, it has been unclear whether Arabidopsis simply responds to WD differently. Our results here show that Arabidopsis does indeed maintain a classical WD response that expands the root system and directs growth downward. Interestingly, under our stress regime, we did not observe a significant decrease in the relative water content of shoot tissues (Figure 6-figure supplement 5), suggesting that the changes in root architecture were sufficient to provide access to deep water and prevent dehydration. Such changes in root growth are likely regulated through systemic and local signaling that involve auxin signaling but acts independently of known pathways that control moisture-directed root growth.

Perspectives and Conclusions.

Understanding plant biology requires a sophisticated understanding of how environmental stimuli affect the form and function of plants as well as an understanding of how physiological context informs such responses. Environmental conditions are at least as complex as the plants they affect. Plant roots are exposed to a variety of environmental signals that change in time and space at very different scales that are integrated at the whole plant system. It is an important challenge in biology to develop methods of growing and studying plants that present such stimuli in a manner that the plant is likely to encounter in nature. After all, the plants we study have evolved to survive through mechanisms that have been selected, over evolutionary time, in nature. It will be interesting for future studies to determine how other environmental stimuli affect root growth using GLO-Roots and whether these responses differ between accessions of Arabidopsis. Identification of the genetic loci responsible for phenotypic variation in adult root phenotypes may identify the molecular basis for adaptive variation that exists in this species and potentially identify loci that are useful for breeding efforts needed for the next green revolution.

Materials and methods.

Growth system.

Rhizotrons and growth system fabrication. Rhizotrons are composed of two sheets of 1/8" abrasion resistant polycarbonate plastic (Makrolon AR (R)) cut to size using a water jet (AquaJet LLC, Salem, OR), two acrylic spacers cut using a laser (Stanford Product Realization Lab), two rubber U-channels cut to strips 30 cm long (McMaster Carr part # 8507K33) and two sheets of black 0.030" thick polypropylene sheets (McMaster Carr part # 1451T21) cut with a straight-edge razor blade. Rhizotron designs were drafted in Adobe Illustrator (Adobe, San José, CA). The blueprints of all the parts are provided in Supplement 1. The top edge of each polycarbonate sheet was painted with black 270 Stiletto nail polish (Revlon, New York, NY).

Boxes and holders. Rhizotrons are held vertical during plant growth in a custom rack system composed of two sheets of 1/4" black acrylic plastic cut with slots for eleven rhizotrons using a laser, four 3/8" PVC rods (McMaster Carr part # 98871a041) secured with PVC nuts (McMaster Carr part # 94806a031) to hold the acrylic sheets horizontal. The rack is placed inside a 12" x 12" x 12" black polyethylene tank (Plastic Mart part # R121212A).

Rhizotron preparation The procedure to construct a rhizotron with soil is as follows: Two pieces of polycarbonate plastic are laid flat on a table with the spacers inserted. Using an electric paint gun, a fine mist of water is applied to the bare polycarbonate sheets. Then, using a 2 mm sieve (US Standard Sieve Series Nº 10) a fine layer of PRO-MIX(r) PGX soil (Premier Tech, Canada) is applied. Excess soil is discarded by gently tapping the plastic against the table in a vertical position. Water is sprayed again onto the soil, then a second layer of Pro-MIX is applied as before. For P deficiency experiments soil supplemented with 1 ml of 100 µM P-Alumina (control) and 0-P-Alumina (P deficient) was used. To prevent the soil from falling out of the bottom opening, a 3 x 6 cm piece of nylon mesh is rolled into a 1 cm wide tube and placed at the bottom side of the rhizotron. The spacers are removed and replaced by clean spacers. The two faces of the rhizotron are carefully joined together and two rubber U-channels slipped on to clamp all pieces together. Assembled rhizotrons are placed into the rack inside the boxes and 500 mL of water is added to the box.

Plant growth *Arabidopsis thaliana* seeds were stratified for 2 d at 4 ºC in Eppendorf tubes with distilled water. Seeds were suspended in 0.1 % agar and 5 to 10 were sown using a transfer pipette in the rhizotron. A transparent acrylic sheet was mounted on top of the box and sealed with tape to ensure high humidity conditions that enable *Arabidopsis* germination. Three days after sowing, the cover was unsealed to decrease humidity and allow the seedlings to acclimate to a dryer environment. From 3 days after sowing (DAS) to the time the first true leaves emerged, it was critical to ensure that the top part of the rhizotron remained humid for proper germination of the plants. Between three and five DAS the rhizotrons were thinned leaving only the number plants required for that experiment, typically one, except for experiments examining root-root interactions. Unless otherwise

stated, all the experiments presented here, treatments were started 10 DAS. Plants were grown under long day conditions (16 h light / 8 h dark) using 20–22 ºC (day/night) and 150 µE m–1 s–1. Two types of growth environments were used for experiments. A walk-in growth chamber with fluorescent lightning and a growth cabinet with white LED lights. Relative water content measurements were done as previously described[36]

qRT-PCR analysis.

Seeds were surface sterilized as described before[2] and grown in rhizotrons, 100 cm^3 pots, or on two types of 1% agar (Duchefa) media containing either 1x MS nutrients (Caisson) and 1% Sucrose, (termed ms media) or ¼x MS nutrients only (termed ms25 media). Both media were buffered using 0.5 g/L MES and pH was adjusted to 5.7 with KOH. All plants were grown together in a growth cabinet with LED lights under long day conditions (16h day/8h night). Root and shoot tissue was collected separately from individual plants at the end of the day (1 hour before the lights shut off) and at the end of the night (1 hour before lights came on). Three biological replicates were collected for each condition. RNA was extracted using the Plant RNA MiniPrepTM kit (ZYMO Research) according to manufacturer's instructions with on-column DNase treatment (Qiagen). cDNA was made using the iScript Advanced cDNA Synthesis for RT-qPCR kit (Bio-Rad) from 200 ng of total RNA. qRT-PCR was performed using a Fluidigm BioMarkTM 96.96 Dynamic Array IFC with the EvaGreen® (Bio-Rad) fluorescence probe according to the Fluidigm Advanced Development Protocol number 37. For the analysis, all the reactions with no amplification (Ct =999) were set to the maximal Ct for that assay type. The two technical replicates were then averaged and dCt values calculated using AT3G07480, AT4G37830, At1g13320 and At1g13440 as reference internal controls. PCA plots were generated with Devium Web[37] using dCt values. dCT values were calculated as dCT = CT~gene interest~ - mean(CT~reference gene~). Primers used are listed in file Supplement 8.

Biological components.

Codon optimization of luciferases. The following luciferases that emit light at different wavelengths were codon optimized for Arabidopsis (Genscript, Piscataway, NJ): LUC2: a yellow improved version (Promega, Madison, WI) of the original *Photinus pyralis* (firefly) LUC.

- Ppy RE8: a red variant[38] of the P. pyralis thermostable variant Ppy RE-TS[39].
- CBG99: a green variant (Promega, Madison, WI) from yellow click beetle (*Pyrophorus plagiophthalamus*) luciferases.
- CBR: a red variant (Promega, Madison, WI) from yellow click beetle.

Non-optimized luciferases. We also used the following non-optimized luciferases:

- nanoLUC: a blue luciferase isolated from a deep sea shrimp[14].
- venusLUC2: a venus-LUC2 fusion reported to show higher luminescence output than LUC2[15].
- A transposon containing the bacterial luciferase-containing LUX operon was integrated into the *Pseudomonas fluorescens* CH267[22] genome by conjugation with *E. coli SM10 pir* containing pUT-EM7-LUX[40] and used to track root microbe colonization. For inoculation 9 DAS plants were inoculated with 2 mL of an overnight bacterial culture resuspended in 10 mM MgSO~4 and diluted to 0.01 OD.

Generation of single-reporter transgenic plants. We generated transcriptional fusions of all luciferases to constitutive promoters to examine the activity level and emission spectrum of each isoform. The *attL1-attL2* entry clones containing plant-codon optimized coding sequence of *LUC2*, *PpyRe8*, *CBG99* and *CBR* were synthesized by Genscript. A DNA fragment including the *UBQ10* promoter region and first intron was amplified from Col–0 genomic DNA with primers incorporating the attB1, attB4 combination sites at the 5'

and 3' respectively. The PCR product was then introduced into pDONR™ P4-P1R (Invitrogen) through a classic Gateway BP-reaction. The resulting plasmid, the *attL1-attL2* entry clones with luciferase sequences, an empty *att*R2-attL3* entry clone and the destination vector dpGreenmCherry[2] were used to construct *ProUBQ10*:LUC2o, *ProUBQ10:PpyRE8o*, *ProUBQ10:CBG99o* and *ProUBQ10:CBRo* through Gateway LR reactions. The destination vector *dpGreenmCherry* contains a plasma membrane-localized mCherry coding sequence driven by the 35S promoter and is used as a selectable marker of transformation at the mature seed stage[2]. We used Golden Gate cloning and the destination vectors that we had generated before[16] for the following fusions: *ProUBQ10:nanoLUC2*, *ProUBQ10*:venusLUC, ProACT2*:PpyRE8o*. Briefly, the different components of each construct were PCR amplified with complementary BsaI or SapI cutting sites, mixed with the destination vector in a single tube, digested with either BsaI or SapI, ligated with T4 DNA ligase, then transformed into E. coli Top10 cells and plated on LB antibiotic plates containing X-gal as previously described[16]. Junction sites were confirmed by sequencing. We used pSE7 (Addgene ID #: pGoldenGate-SE7: 47676) as the destination vector of the *ProUBQ10:nanoLUC2*, *ProUBQ10:venusLUC* constructs and pMYC2 (Addgene ID #: pGoldenGate-MCY2: 47679) as the destination vector for *ProACT2:PpyRE8o*. Maps of all the vectors can be found in Supplement 8. *ProUBQ10:LUC2o* was transformed into Col-0, Bay and Sha accessions, the *tir1-1*[41] mutant and the *miz1*[42] T-DNA insertion line (SALK_126928).

Brachypodium distachyon. The Arabidopsis plant-codon optimized Luciferase gene, *LUC2o*, was inserted into the monocot vector pANIC10 *via* Gateway cloning[31]. *Brachypodium distachyon* plants were transformed using the method of Vogel and Hill[43].

Tomato. The transcriptional fusion *ProeDR5:LUC2* was generated by cloning the *ProeDR5:LUC2* DNA fragment into the pBIB expression vector via restriction sites SalI and Acc65I. The eDR5 promoter is an enhanced version of DR5 containing 13 repeats of the 11-nucleotide core DR5 element[44] and the pBIB expression vector contains an NPTII resistance gene under the control of the NOS promoter for use as a selectable marker during

transformation. All tomato transformations were performed by the Ralph M. Parsons Foundation Plant Transformation Facility (University of California, Davis).

Generation of dual-reporter plants. To generate dual-reporter plants expressing luciferase isoforms that emit light with divergent emission spectra we used *ProACT2:PpyRE8o* as the root structural marker and ZAT12:LUC[21] and DR5:LUC+[20] lines that were transformed with the *ProACT2:PpyRE8o* construct. All constructs were transformed using a modified floral dip method as described in[2].

To make the dual color tomato plants, the *Pro35S:PpyRE8o* transcriptional fusion was generated by putting the plant-codon optimized coding sequence described above into the pMDC32 expression vector through a Gateway LR reaction. The pMDC32 vector contains a hygromycin resistance gene under the control of the 35S promoter for use as a selectable marker during transformation. This construct was transformed into the transgenic *ProeDR5:LUC2* tomato line.

In vivo emission spectra of plants constitutively expressing luciferase isoforms. To generate *in vivo* emission spectra of all constitutively expressed luciferases, seeds were sterilized and sown on MS plates as described before[2]. After 8 days, seedlings were treated with a 100 µM luciferin solution, incubated at room temperature for 3 hours and imaged using an IVIS Spectrum imaging system (Perkin Elmer, Waltham , MA) using 20 nm bandpass emission filters at the following wavelengths (in nm: 490-510, 510-530, 530-550, 550-570, 570-590, 590-610, 610-630, 630-650, 650-670, 670-690, 690-710). Raw images were analyzed using Fiji and in vivo emission spectra were constructed. The full emission spectra of LUX and nanoLUC could not be constructed since the maximum of these two luciferases is below the lower band pass filter that were available.

Imaging system. We designed a custom imaging system (GLO1, Growth and Luminescence Observatory 1) optimized for imaging dual-reporter luciferase expression in our custom rhizotrons. The design was a joint effort with Bioimaging Solutions (San Diego, CA) who

also built the system and wrote the acquisition software that drives all the mechanical parts of the system. The system is composed by two 2048 x 2048 PIXIS-XB cameras (Princeton Instruments, Trenton, NJ) mounted on top of each other to capture two fields of view encompassing approximately two 15 x 15 cm areas corresponding to the top or bottom of the rhizotron. The cameras are fitted with a Carl-Zeiss macro lens. A filter wheel with space for four, 76.2 mm filters is positioned in front of the cameras and controlled by a stepper motor allowing for automated changing of the filter wheel position. We used two -542/50 and 450/70- custom cut Brightline(R) band-pass filters (Semrock, Rochester, NY). In single color imaging mode, the filter wheel is operated without filters. Positioned in front of the filter wheel is a removable rhizotron holder mounted on a stepper motor. This stepper motor is also controlled by the GLO-1 software allowing automatic acquisition of images from both sides of the rhizotron sequentially. The whole imaging system is enclosed in a light-tight black box with a door that allows loading and un-loading of rhizotrons.

Plant Imaging. Around 50 mL of 300 µM D-luciferin (Biosynth, Itasca, IL) was added to soil at the top of the rhizotron. In general 5 min exposures were taken per rhizotron, per side, per channel. For daily imaging experiments, plants were imaged at dawn (+/- 1 hr) to reduce possible effects on diurnal rhythms of keeping plants in the dark during imaging. Shoot images were taken using a Nikon D3100 camera.

Image Preparation. Four individual images are collected: top front, bottom front, top back and bottom back. Using an automated ImageJ macro, a composite image is generated as follows: 1)To correct for differences in background values between the two cameras the mean background value of each image is subtracted from 200; 2) images are rotated and translated to control for small misalignments between the two cameras; 3) the top and bottom images of each side are merged; 4) the back image is flipped horizontally; 5) the front and back images are combined using the maximum values. When dual color images are acquired this operation is repeated for each channel. The final images produced are 16-bit depth and 4096 x 2048 pixels. The scale of the images is 138.6 pixels per cm. Considering

that an Arabidopsis roots is 100 µm this results in 1.39 pixels across an Arabidopsis root.

GLO-RIA imageJ plug-in. GLO-RIA uses a combination of existing tools to extract relevant root architecture features. Directionality is acquired using the directionality plugin from ImageJ. After the number of direction bins (we usually use bins of 2º) is defined by the user, a 5x5 sobel operator is used to derive the local gradient orientation. This orientation is then used to build a distribution of directions by assigning the square of the orientation into the appropriate bin. Instead of representing the total counts at each orientation a relative value is calculated by dividing the individual values at each bin by the total sum of the histogram (and multiplying by 100). Similar algorithms have been used to quantify dynamic changes in the plant cytoskeleton[45].

The Elliptic Fourier Descriptors are aquired using the Fourier Shape Analysis plugin on convex hull shape of the root system. Elliptic Fourier Descriptors have been used in numerous studies to analyse variations in shapes, notably in leaves (e.g[46]).

The shape analysis is inspired by RootScape[17]. Due to the absence of fixed, recognisable structures in root system (that are required for the position of true landmarks), pseudo-landmarks are automatically extracted from the root systems. Shortly, the image is divided vertically at equidistant positions (with the number defined by the user) and for each of the image stripes, the minimum and maximum x coordinates are computed. The shape analysis is therefore able to discriminate root system with different vertical root distributions or global root system orientation (e.g. chemotropism) . The code source for the plugin, manual and sample images can be found in the github repository of the project.

Statistical analysis was performed in R[48]. The tidyr[49], dplyr[49], gridExtra[50], shapes[51], geomorph[52], ggplot2[53] and cowplot[54] packages were used for data preparation, analysis and plotting. Final figure preparation was done in Inkscape.

Data availability. All the scripts and original data used to analyze and produce the images can be accessed in the Github repository of the project: github.com/rr-lab/GLO-Roots. Raw files of all the images used in the paper are availabe in Dryad.

Acknowledgements.

Work in the lab of JRD was funded by the Carnegie Institution for Science Endowment and grants from the National Science Foundation (MCB-115795) and Department of Energy, Biological and Environmental Research program (DE-SC0008769). RRA was supported by a Carnegie Postdoc Fellowship and currently by Conacyt Ciencia Básica Joven Investigador grant number (CB-2014-01-238101). GL was supported by the Belgian Fonds de la Recherche Scientifique. JM was funded by the National Science Foundation (IOS-0820854). CH is funded by MGH Toteston & Fund for Medical Discovery Fellowship grant 2014A051303 and NIH R37 grant GM48707 and NSF grant MCB-0519898 awarded to Frederick Ausubel, and previously by the Gordon and Betty Moore Foundation through Grant GBMF 2550.01 from the Life Sciences Research Foundation. JV was funded by the Office of Biological and Environmental Research, Office of Science, US Department of Energy, interagency agreements DE-SC0001526 and DE-AI02-07ER64452. We thank Robert Mittler and Philip Benfey for providing seeds of ZAT12:LUC and DR5:LUC+ respectively.

We also thank Neil Robbins and members of the Dinneny lab for critical review of the manuscript and suggestions during the development of the project. We greatly appreciate Tim Doyle at the Stanford Small Animal Imaging Facility for providing advice in the use of luciferase-based imaging approaches.

Competing interests.

We do not have any competing interests that we are aware of.

References

1.Dinneny, J. R. *et al.* Cell identity mediates the response of *Arabidopsis* roots to abiotic stress. *Science* **320,** 942–945 (2008).

2.Duan, L. *et al.* Endodermal ABA Signaling Promotes Lateral Root Quiescence during Salt Stress in Arabidopsis Seedlings. *Plant Cell* **25,** 324–341 (2013).

3.Lynch, J. P. & Wojciechowski, T. Opportunities and challenges in the subsoil: pathways to deeper rooted crops. *J. Exp. Bot.* **66,** 2199–2210 (2015).

4.Brady, N. C. & Weil, R. R. *Elements of the nature and properties of soils.* (Prentice Hall, 2009).

5.Bao, Y. *et al.* Plant roots use a patterning mechanism to position lateral root branches toward available water. *Proc Natl Acad Sci* **111,** 9319–9324 (2014).

6.Tabata, R. *et al.* Perception of root-derived peptides by shoot LRR-RKs mediates systemic N-demand signaling. *Science* **346,** 343–346 (2014).

7.Rosquete, M. R. *et al.* An Auxin Transport Mechanism Restricts Positive Orthogravitropism in Lateral Roots. *Current Biology* **23,** 817–822 (2013).

8.Uga, Y. *et al.* Control of root system architecture by DEEPER ROOTING 1 increases rice yield under drought conditions. *Nat. Genet.* **45,** 1097–1102 (2013).

9.Postma, J. A. & Lynch, J. P. The optimal lateral root branching density for maize depends on nitrogen and phosphorus availability. *Plant Physiol.* **166,** 590–602 (2014).

10.Laliberté, E. *et al.* How does pedogenesis drive plant diversity? *Trends in ecology & evolution* **28,** 331–340 (2013).

11.Tian, H., De Smet, I. & Ding, Z. Shaping a root system: regulating lateral versus primary root growth. *Trends in plant science* **19,** 426–431 (2014).

12.Schneider, C. A., Rasband, W. S. & Eliceiri, K. W. NIH Image to ImageJ: 25 years of image analysis. *Nature methods* **9,** 671–675 (2012).

955 13.Meijon, M., Satbhai, S. B., Tsuchimatsu, T. & Busch, W. Genome-wide association study
956 using cellular traits identifies a new regulator of root development in. *Nat. Genet.* **46,** 77–81
957 (2013).

958 14.Hall, M. P. *et al.* Engineered Luciferase Reporter from a Deep Sea Shrimp Utilizing a
959 Novel Imidazopyrazinone Substrate. *ACS chemical biology* **7,** 1848–1857 (2012).

960 15.Hara-Miyauchi, C. *et al.* Bioluminescent system for dynamic imaging of cell and animal
961 behavior. *Biochem. Biophys. Res. Commun.* **419,** 188–193 (2012).

962 16.Emami, S., Yee, M.-C. & Dinneny, J. R. A robust family of Golden Gate Agrobacterium
963 vectors for plant synthetic biology. *Front. Plant Sc.* **4,** 339 (2013).

964 17.Ristova, D. *et al.* RootScape: a landmark-based system for rapid screening of root
965 architecture in Arabidopsis. *Plant Physiology* **161,** 1086–1096 (2013).

966 18.Lobet, G. *et al.* Root System Markup Language: toward a unified root architecture
967 description language. *Plant Physiol.* **167,** 617–627 (2015).

968 19.Pagès, L. *et al.* Calibration and evaluation of ArchiSimple, a simple model of root system
969 architecture. *Ecological Modelling* **290,** 76–84 (2014).

970 20.Moreno-Risueno, M. A. *et al.* Oscillating gene expression determines competence for
971 periodic *Arabidopsis* root branching. *Science* **329,** 1306–1311 (2010).

972 21.Miller, G. *et al.* The plant NADPH oxidase RBOHD mediates rapid systemic signaling
973 in response to diverse stimuli. *Science Signaling* **2,** ra45 (2009).

974 22.Haney, C. H., Samuel, B. S., Bush, J. & Ausubel, F. M. Associations with rhizosphere
975 bacteria can confer an adaptive advantage to plants. *Nature Plants* **1,** 15051 (2015).

976 23.Mandoli, D. F., FORD, G. A., WALDRON, L. J., NEMSON, J. A. & Briggs, W. R. Some
977 spectral properties of several soil types: implications for photomorphogenesis*. *Plant Cell*
978 *Environ.* **13,** 287–294 (1990).

979 24.Galen, C., Rabenold, J. J. & Liscum, E. Functional ecology of a blue light photoreceptor:
980 effects of phototropin-1 on root growth enhance drought tolerance in Arabidopsis thaliana.

New Phytol. **173,** 91–99 (2007).

25.Moni, A., Lee, A. Y., Briggs, W. R. & Han, I. S. The blue light receptor Phototropin 1 suppresses lateral root growth by controlling cell elongation. *Plant Biology* 34–40 (2014).

26.Yokawa, K., Kagenishi, T. & Baluška, F. Root photomorphogenesis in laboratory-maintained Arabidopsis seedlings. *Trends Plant Sci.* **18,** 117–119 (2013).

27.Lobell, D. B. *et al.* Greater Sensitivity to Drought Accompanies Maize Yield Increase in the U.S. Midwest. *Science* **344,** 516–519 (2014).

28.Ort, D. R. & Long, S. P. Limits on Yields in the Corn Belt. *Science* **344,** 484–485 (2014).

29.Pacheco-Villalobos, D. & Hardtke, C. S. Natural genetic variation of root system architecture from Arabidopsis to Brachypodium: towards adaptive value. *Philosophical Transactions of the Royal Society of London B: Biological Sciences* **367,** 1552–1558 (2012).

30.Watt, M., Schneebeli, K., Dong, P. & Wilson, I. W. The shoot and root growth of Brachypodium and its potential as a model for wheat and other cereal crops. *Functional Plant Biol.* **36,** 960–969 (2009).

31.Mann, D. G. J. *et al.* Gateway-compatible vectors for high-throughput gene functional analysis in switchgrass (Panicum virgatum L.) and other monocot species. *Plant Biotechnol. J.* **10,** 226–236 (2012).

32.Pacheco-Villalobos, D., Sankar, M., Ljung, K. & Hardtke, C. S. Disturbed Local Auxin Homeostasis Enhances Cellular Anisotropy and Reveals Alternative Wiring of Auxin-ethylene Crosstalk in Brachypodium distachyon Seminal Roots. *PLoS Genet* **9,** e1003564 (2013).

33.Buer, C. S., Wasteneys, G. O. & Masle, J. Ethylene modulates root-wave responses in Arabidopsis. *Plant Physiology* **132,** 1085–1096 (2003).

34.Blossfeld, S., Schreiber, C. M., Liebsch, G., Kuhn, A. J. & Hinsinger, P. Quantitative imaging of rhizosphere pH and CO2 dynamics with planar optodes. *Annals of Botany* **112,** 267–276 (2013).

35.Shaw, S. L. & Ehrhardt, D. W. Smaller, Faster, Brighter: Advances in Optical Imaging of Living Plant Cells. *Annu. Rev. Plant Biol.* **64,** 351–375 (2013).

36.Barr, H. & Weatherley, P. A re-examination of the relative turgidity technique for estimating water deficit in leaves. *Aust. J. Biol. Sci* **15,** 413–428 (1962).

37.Grapov, D. DeviumWeb: Dynamic Multivariate Data Analysis and Visualization Platform.

38.Branchini, B. R. *et al.* Red-emitting luciferases for bioluminescence reporter and imaging applications. *Analytical Biochemistry* **396,** 290–297 (2010).

39.Branchini, B. R. *et al.* Thermostable red and green light-producing firefly luciferase mutants for bioluminescent reporter applications. *Analytical Biochemistry* **361,** 253–262 (2007).

40.Lane, M. C., Alteri, C. J., Smith, S. N. & Mobley, H. L. T. Expression of flagella is coincident with uropathogenic Escherichia coli ascension to the upper urinary tract. *Proc. Natl. Acad. Sci. U.S.A.* **104,** 16669–16674 (2007).

41.Ruegger, M. *et al.* The TIR1 protein of Arabidopsis functions in auxin response and is related to human SKP2 and yeast grr1p. *Genes Dev* **12,** 198–207 (1998).

42.Moriwaki, T. *et al.* Hormonal Regulation of Lateral Root Development in Arabidopsis Modulated by MIZ1 and Requirement of GNOM Activity for MIZ1 Function. *Plant Physiol.* **157,** 1209–1220 (2011).

43.Vogel, J. & Hill, T. High-efficiency Agrobacterium-mediated transformation of Brachypodium distachyon inbred line Bd21-3. *Plant Cell Rep* **27,** 471–478 (2008).

44.Covington, M. F. & Harmer, S. L. The Circadian Clock Regulates Auxin Signaling and Responses in Arabidopsis. *Plos Biol* **5,** e222 (2007).

45.Lindeboom, J. J. *et al.* A Mechanism for Reorientation of Cortical Microtubule Arrays Driven by Microtubule Severing. *Science* **342,** 1245533–1–1245533–11 (2013).

1032 46.Chitwood, D. H. *et al.* A modern ampelography: a genetic basis for leaf shape and
1033 venation patterning in grape. *Plant Physiology* **164,** 259–272 (2014).

1034 47.Iwata, H. & Ukai, Y. SHAPE: a computer program package for quantitative evaluation of
1035 biological shapes based on elliptic Fourier descriptors. *The Journal of Heredity* **93,** 384–385
1036 (2002).

1037 48.R Core Team. *R: A language and environment for statistical computing*. (R Foundation
1038 for Statistical Computing, 2014). at <http://www.R-project.org/>

1039 49.Wickham, H. *Tidyr: Easily tidy data with spread() and gather() functions*. (2014). at
1040 <http://CRAN.R-project.org/package=tidyr>

1041 50.Auguie, B. *GridExtra: Functions in grid graphics*. (2012). at <http://CRAN.R-project.
1042 org/package=gridExtra>

1043 51.Dryden, I. L. *Shapes: Statistical shape analysis*. (2013). at <http://CRAN.R-project.
1044 org/package=shapes>

1045 52.Adams, D. & Otarola-Castillo, E. Geomorph: An r package for the collection and analysis
1046 of geometric morphometric shape data. *Methods in Ecology and Evolution* **4,** 393–399 (2013).

1047 53.Wickham, H. *Ggplot2: Elegant graphics for data analysis*. (Springer New York, 2009).
1048 at <http://had.co.nz/ggplot2/book>

1049 54.Wilke, C. O. *cowplot: Streamlined Plot Theme and Plot Annotations for ggplot2*. (2015).
1050 at <http://cran.r-project.org/web/packages/cowplot/index.html>

Videos

Video 1 Time lapse from 11 to 21 DAS of a Col-0 plant expressing ProUBQ10:LUC2o grown in control conditions

Video 2 Time lapse from 16 to 24 DAS of Col-0 plants expressing *ProUBQ10:LUC2o* growing in water deficient (left) and control (right) conditions. Plants were sown under control conditions and water deficit treatment started 11 DAS. Images were taked every day.

Supplementary figures

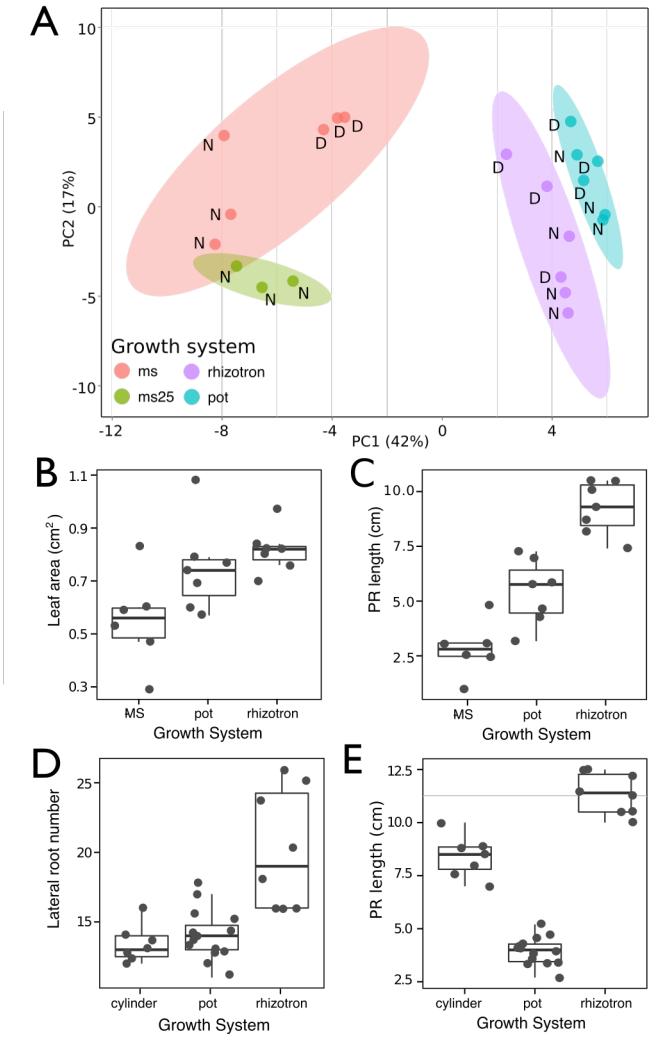

Figure 1-figure supplement 1. Effect of different growth systems on plant biology. A) Principal Components Analysis (PCA) score plot of a set of 76 genes analyzed by qPCR from root samples of plants grown in MS plates, pots, and rhizotrons. After 15 DAS three plants were collected at the end of the day (D) and three were collected at the end of the night (N). (ms = plant grown in full ms and 1% sucrose, ms25 = plants grown in 25% of full ms) B) Lateral root number and G) primary root length of 18 DAS plants grown in 30 cm tall cylinders, pots and rhizotrons, all with a volume of 100 cm^3 (n = 6-12 plants). D) Leaf area and E) primary root length of plants of the same age (15 DAS) as the ones

814 used for the qPCR experiment (n= 6-7). ANOVA analysis with $p < 0.01$ was used to test
815 significant differences between the different parameters.

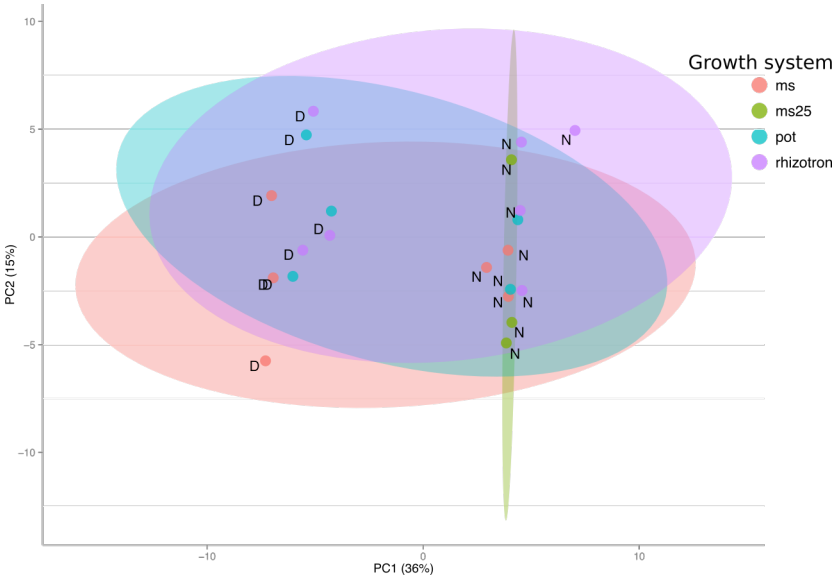

*Figure 1-figure supplement 2. PCA plot of shoots of the same samples analyzed in Figure 1. See Figure 1 for more details regarding experimental conditions used.

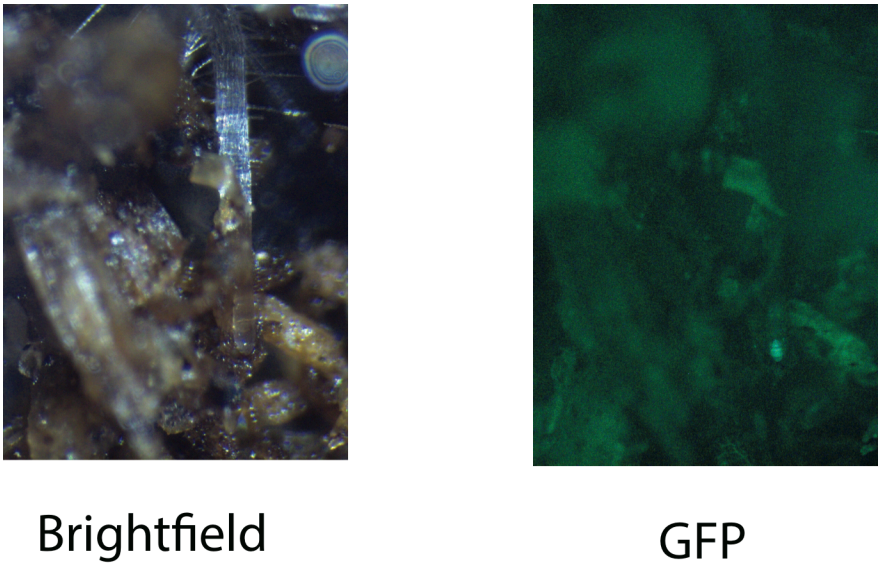

Figure 1-figure supplement 3 Image of an Arabidopsis root in soil imaged with white light (brightfield) or epifluorescence.

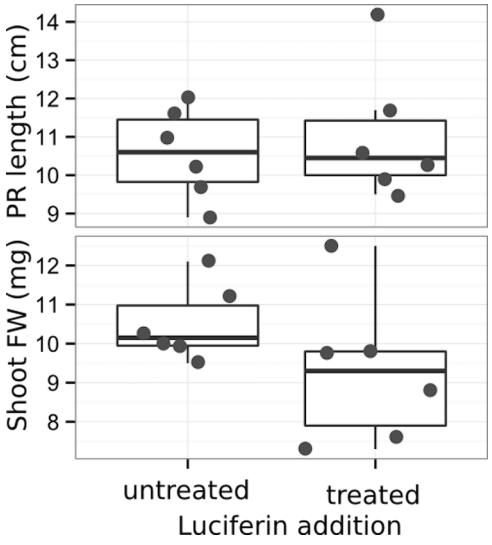

Figure 1-figure supplement 4 Effect of luciferin addition on primary root length and shoot size of 14 DAS seedlings that were either continuously exposed to 300 µM luciferin from 9 DAS after sowing or not.

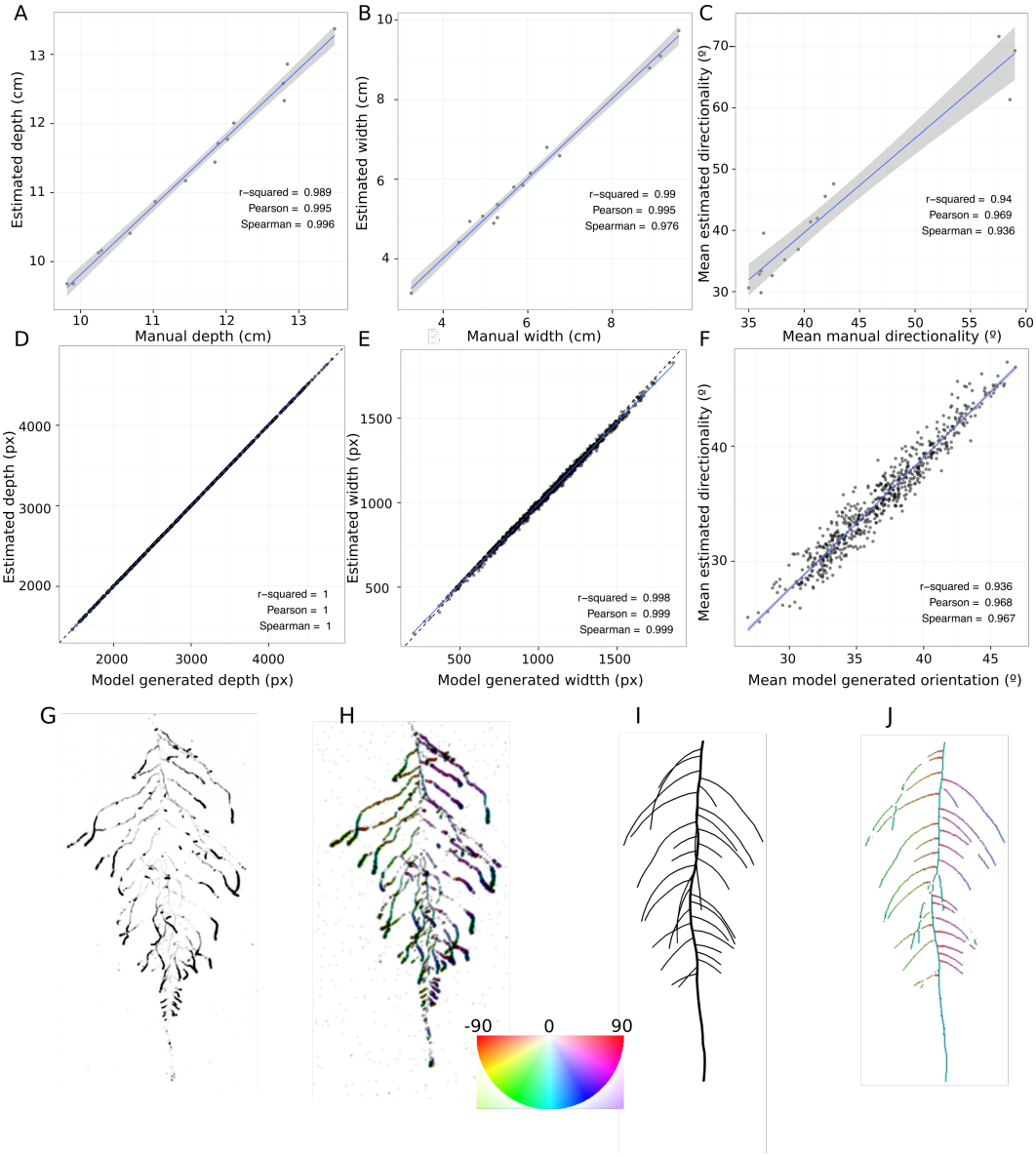

Figure 1-figure supplement 5 GLO-RIA ground truth comparison. Tests of GLO-RIA were performed using two approaches. We first manually quantified root system depth (A) width (B) and average lateral root angle (C) in a set of 15 root systems corresponding to different Arabidopsis accessions. We also generated 1240 contrasting root systems using ArchiSimple and quantified root system depth (D) width (E) and directionality (F) using GLO-RIA. Example of a real (G) and ArchiSimple generated (H) root system

833 and corresponding GLO-RIA determined directionality color-coded into the image (I, J).

834 Absolute orientation angle values are taken before all calculations.

Figure 1-figure supplement data 1: Two way ANOVA P-values comparing plants grown in MS media vs. plants grown in soil (pots or rhizotrons) and plants collected at day or night. We used p-value < 0.00065 threshold based on Bonferoni adjustment for multiple testing.

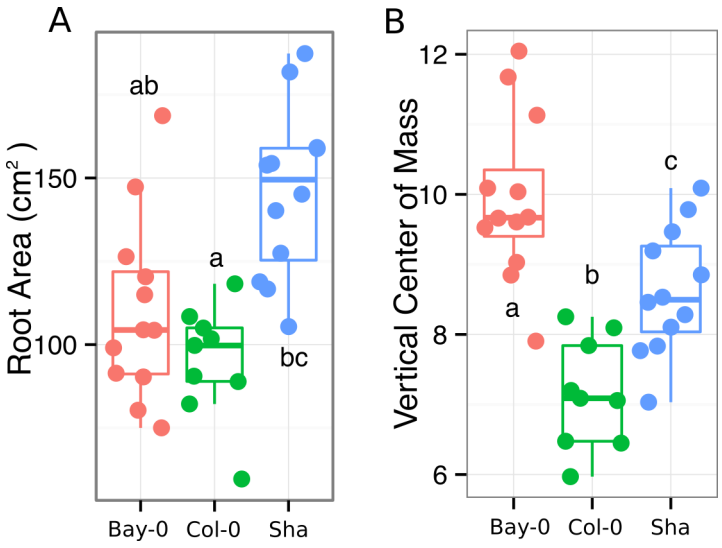

Figure 3-figure supplement 1 A) root area, B) vertical center of mass of Bay-0, Col-0 and Sha accessions.

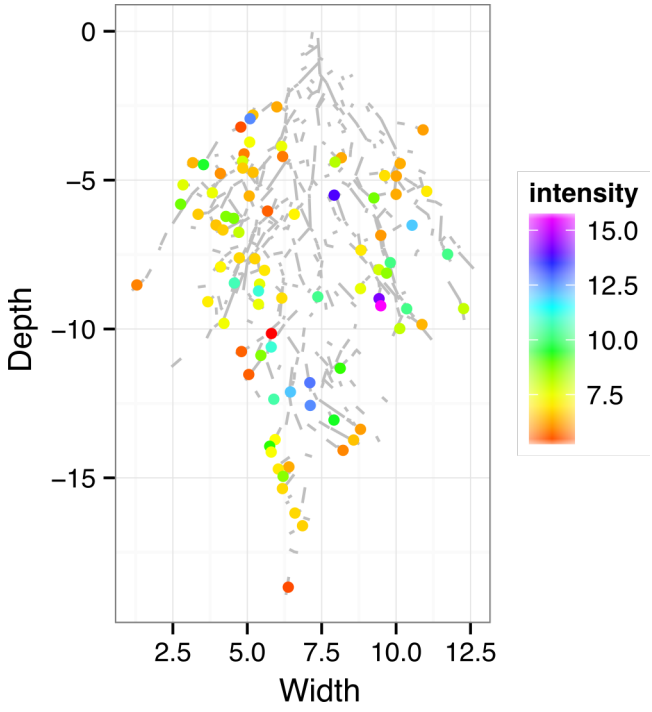

Figure 4-figure supplement 1: ZAT12:LUC intensity and root segments automatically identified with GLO-RIA.

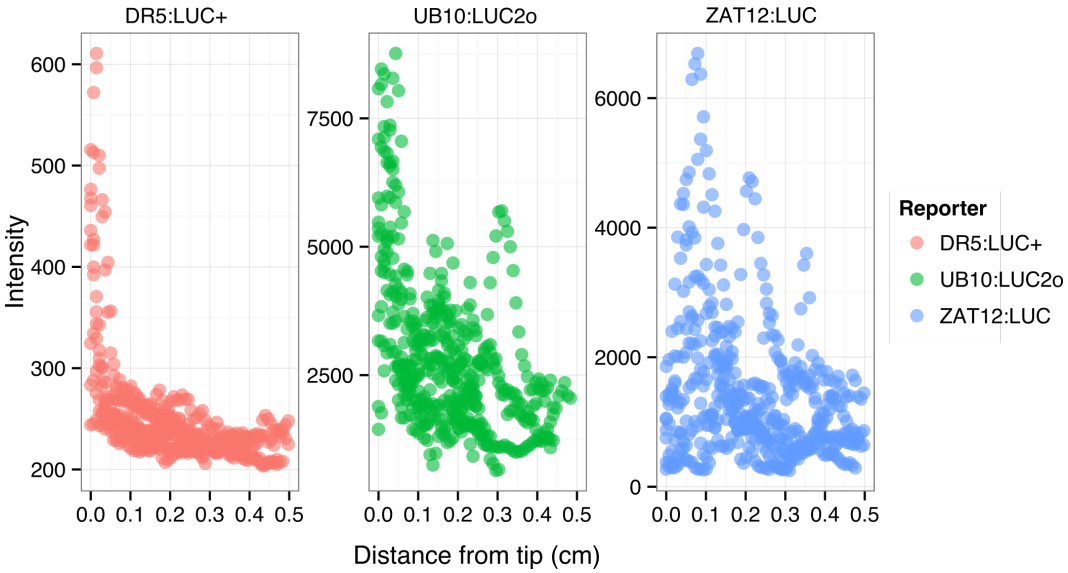

Figure 4-figure supplement 2: DR5:LUC+, UBQ10:LUC2o and ZAT12:LUC intensity values along the root tip. Data was manually obtained by obtaining the intensity profile of the first 0.5 cm from the root tip of individual lateral roots. Ten lateral roots for each reporter were measured.

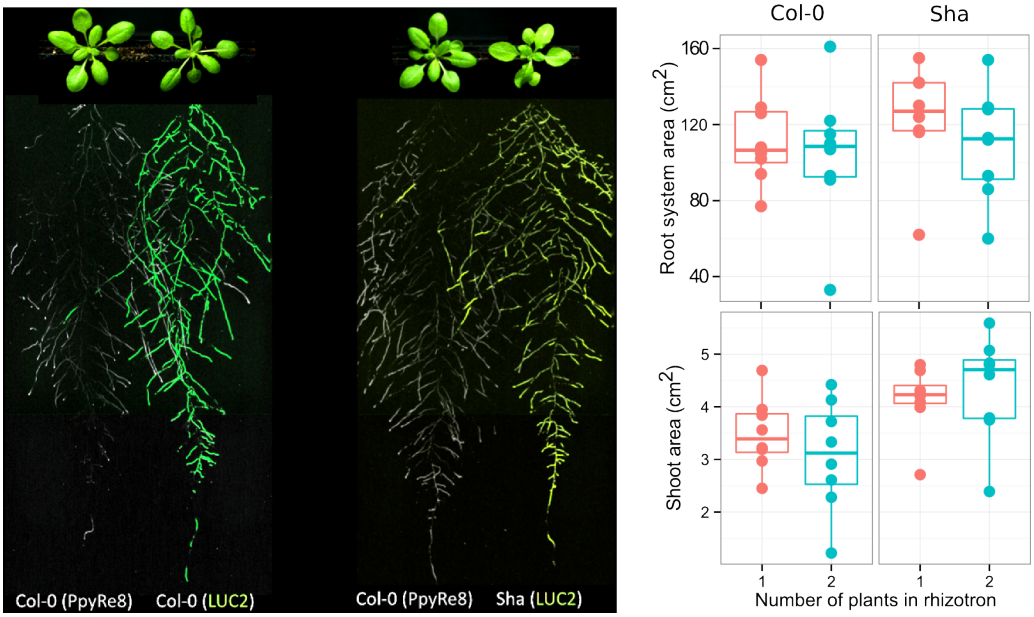

Figure 4-figure supplement 3. Images of plants at 22 DAS growing in the same rhizotron and expressing different luciferases. A) Two Col-0 plants expressing *ProUBQ10:LUC2o* and *ProACT2:PPyRE8o* B) Col-0 plant expressing *ProACT2:PPyRE8o* and Sha plant expressing *ProUBQ10:LUC2o*.

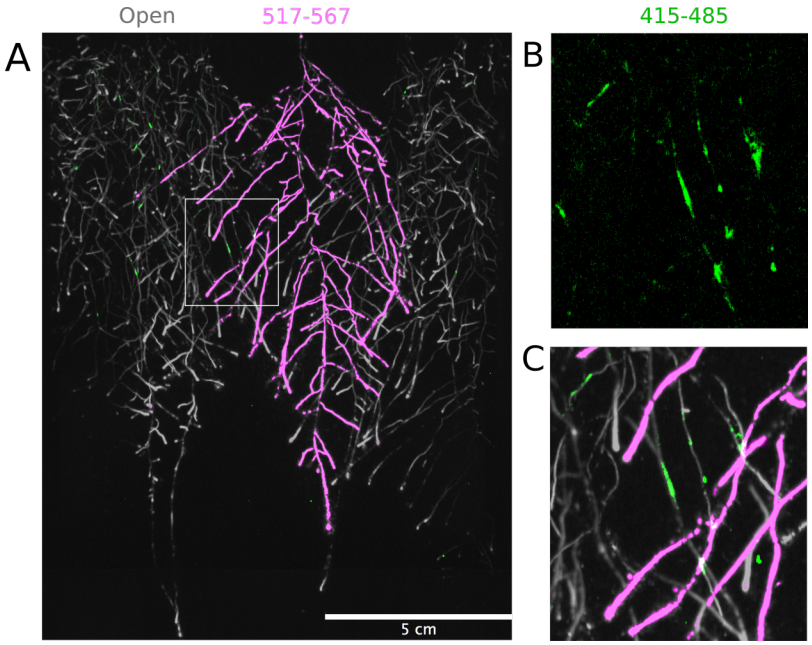

Figure 4-figure supplement 4. Three-reporter-based analysis of root-root-microbe interactions. A) Image showing a 22 DAS *ProUBQ10:LUC2o* plant (magenta) grown in the same rhizotron with *ProACT2:PpyRE8o* plants (grey). Plants were inoculated with *Pseudomonas fluorescens CH267* (green). Magnified portion of root systems colonized by *Pseudomonas fluorescens* showing *P. fluorescences* (B) only or all three reporters together (C).

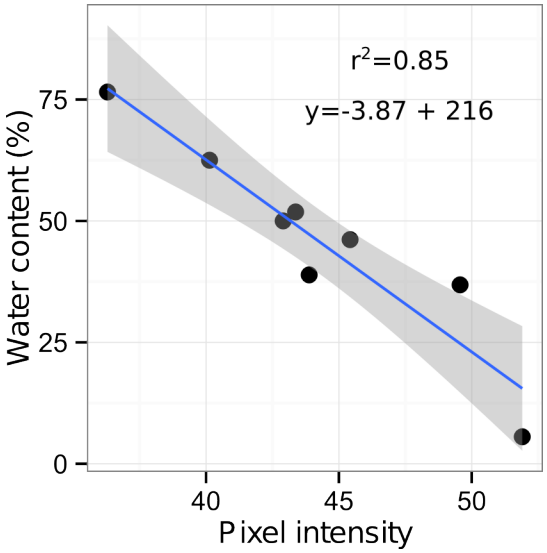

Figure 5-figure supplement 1: Moisture calibration curve. Rhizotrons with different levels of moisture were prepared and scanned to obtain readings of pixel intensity. Soil from rhizotrons was then weighed, dried down in an oven at 70 ºC for 48 hours and percent water content quantified.

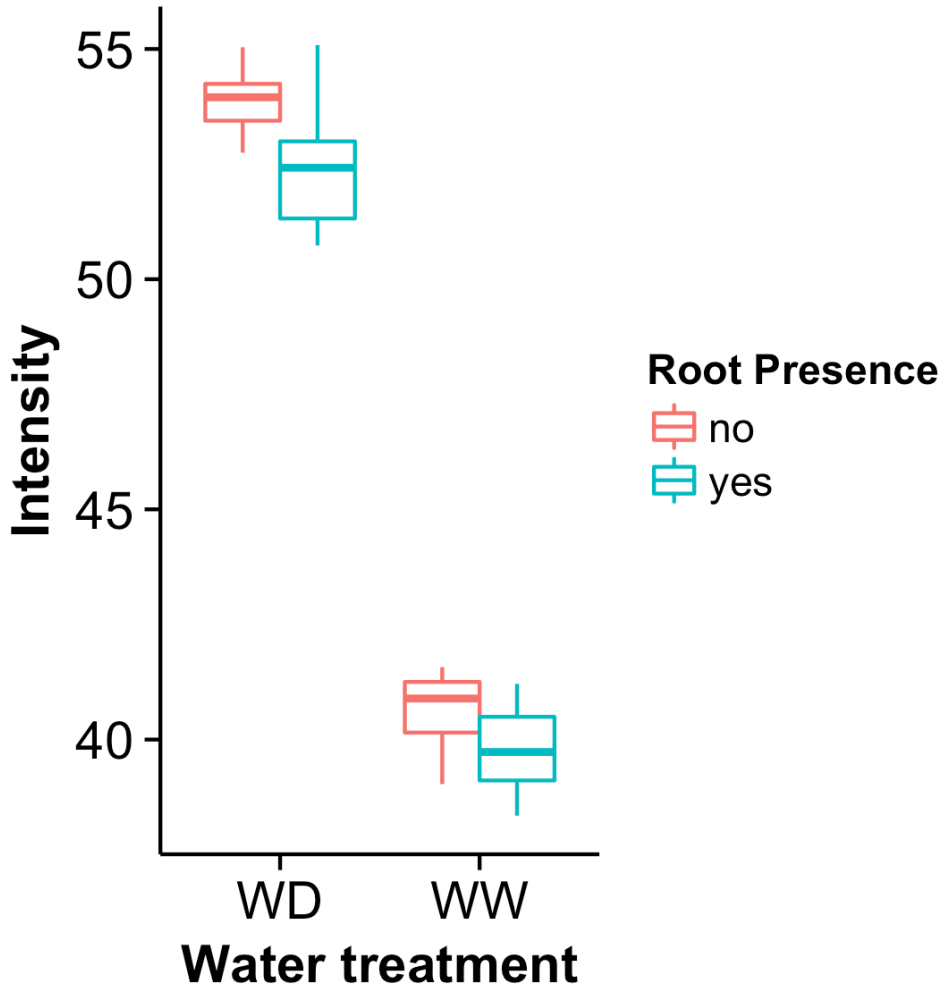

869

870 **Figure 5-figure supplement 2. Comparison of soil intensity values between**
871 **areas of the rhizotron with or without the presence of roots, determined based**
872 **on luminescence data.** Mean intensity values from 100 x 100 pixel squares samples of
873 both areas were obtained from 10 different rhizotrons. Wilcoxon test analysis with $p < 0.01$
874 was used to test significant differences between areas with our without root presence.

875

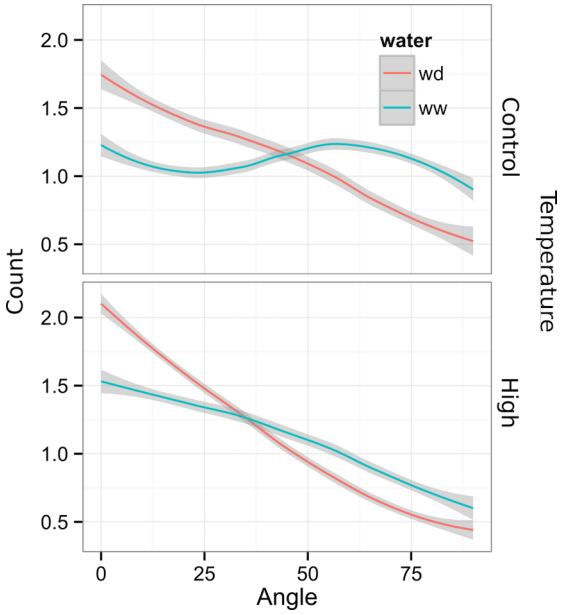

Figure 6-figure supplement 1 Directionality analysis of roots of plants transferred to water deprivation conditions after 9 DAS and kept 22 ºC (control temperature) and 29 ºC (high temperature) until 22 DAS. (0º is the direction of the gravity vector).

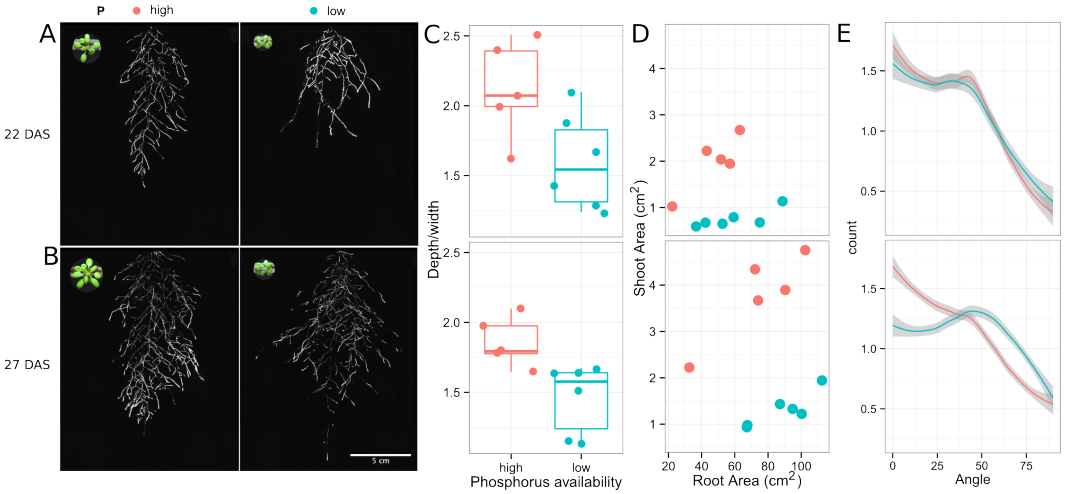

Figure 6-figure supplement 2. Phosphorus deficiency response of root systems Shoot and root systems of *ProUBQ10:LUC2o* Col-0 plants growing in soil supplemented with 1ml of 100 µM P-Alumina (left) and 0-P-Alumina (right) 22 (A) or 27 (B) DAS. C) Root depth/width ratio of 22 (top) and 27 (bottom) DAS plants. D) Scatter-plot showing relationship between root and shoot system area at 22 (top) and 27 (bottom) DAS. E) Root directionality distribution in plants 22 (top) and 27 (bottom) DAS. Anova analysis at $p < 0.01$ was used to compare depth/width ratios in P treatments. Kolmogorov-Smirnov test at $p < 0.001$ was used to compare directionality distributions between the different treatments. A Local Polynomial Regression Fitting with 95% confidence interval (grey) was used to represent the directionality distribution curve.(0^o is the direction of the gravity vector).

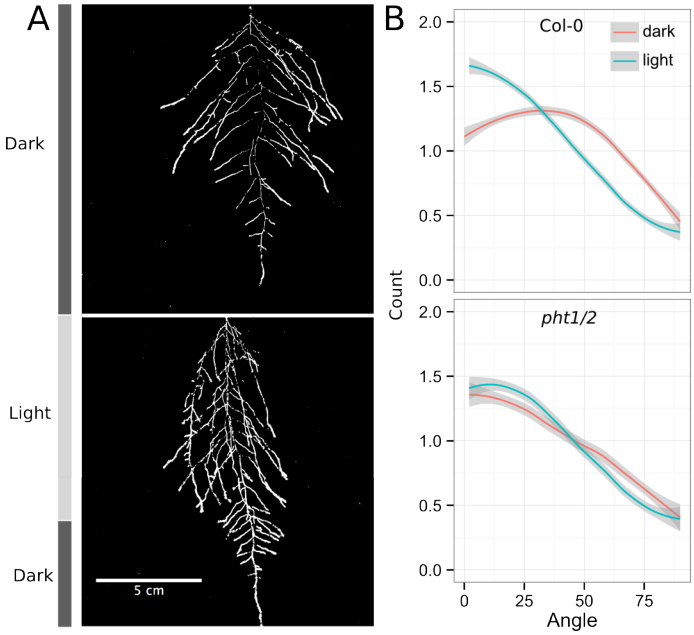

Figure 6-figure supplement 3. Effect of light on root directionality. A) Col-0 root systems shielded (top) or light exposed (bottom). After 9 DAS the top third of the rhizotron was exposed to light (indicated on the side with a light grey bar) and plants were imaged at 20 DAS. B) Directionality analysis of root systems shielded (red) or exposed (green) to light for Col-0 (top panel) or *phot1/2* double mutant (bottom panel). Between 4 and 6 plants were analyzed per treatment. ANOVA analysis at $p < 0.01$ was used to compare depth/width ratios in P treatments. Kolmogorov-Smirnov test at $p < 0.001$ was used to compare directionality distributions between the different treatments. A Local Polynomial Regression Fitting with 95% confidence interval (grey) was used to represent the directionality distribution curve.(0^o is the direction of the gravity vector).

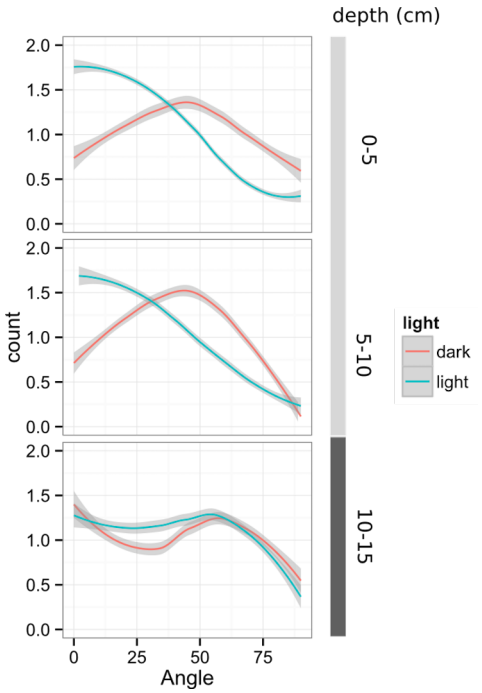

Figure 6-figure supplement 4 Plots showing output of directionality analysis performed at different depths (0-5, 5-10, 10-15 cm) in rhizotrons exposed to light or kept in the dark. (0^o is the direction of the gravity vector).

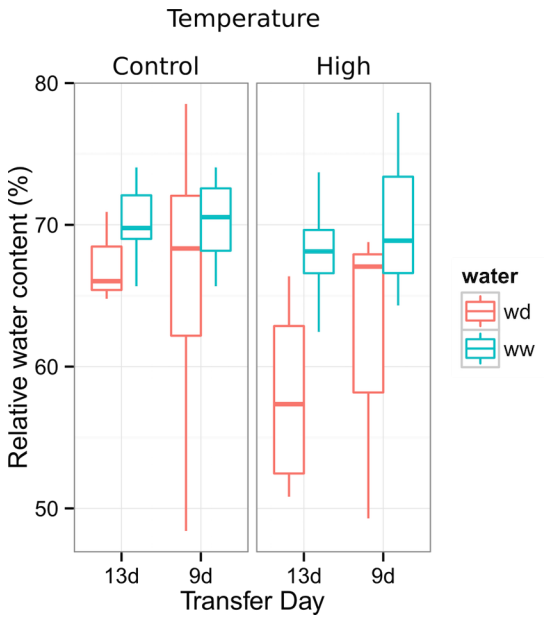

Figure 6-figure supplement 5. Leaf relative water content of 23 DAS plants that were subjected to water deprivation (WD) after 9 or 13 DAS or kept under well watered (WD) conditions. At 9 DAS half of the plants were kept under control temperature conditions (22 ºC) and the other half transferred to a 29 ºC (high) chamber. n = 6-8 plants.

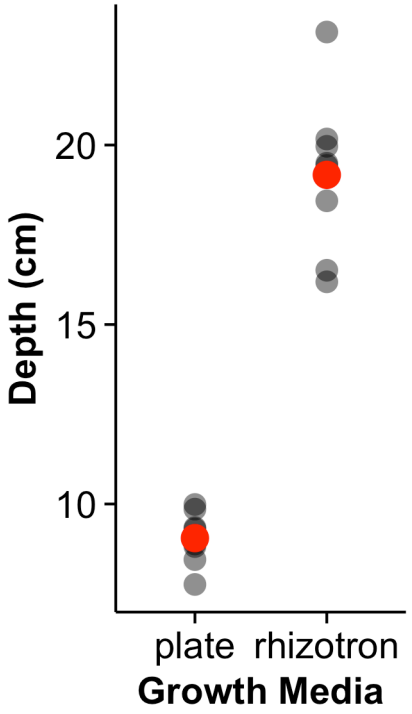

Figure 8-figure supplement 1 Depth of the primary root of Brachypodium plants grown in rhizotrons or on gel-based media (n=8-11). Red dots indicate mean values.

Supplementary material

Supplemental Material 1

Blueprints of the holders, clear sheets and spacers needed to built the rhizotrons. Additional details are provided in the materials and methods. Files are provided in Adobe Illustrator .ai and Autocad .dxf formats.

Supplemental Material 2

Primers used in the qPCR experiment.

Supplemental Material 3

Vector maps of all the constructs used in this work.